

A STUDY OF THE EFFECT OF N-BUTYL ACETATE ON A MOTOR AND GEAR REDUCER SYSTEM FOR A DEEP ICE CORING DRILL

Åsa Hagberg, Torbjörn Henriksson

**University of Luleå
S-95187 Luleå, SWEDEN**



**Polar Ice Coring Office (PICO)*
University of Alaska Fairbanks
Fairbanks, Alaska 99775-1710**

**PICO
TR-90-4**

December 1990

*** PICO is operated by the University of Alaska Fairbanks under contract to the National Science Foundation, Division of Polar Programs.**

**A STUDY OF THE EFFECT OF
N-BUTYL ACETATE ON A
MOTOR AND GEAR REDUCER SYSTEM FOR A
DEEP ICE CORING DRILL**

Åsa Hagberg, Torbjörn Henriksson

**University of Luleå
S-95187 Luleå, SWEDEN**

**Polar Ice Coring Office (PICO)*
University of Alaska Fairbanks
Fairbanks, Alaska 99775-1710**

**PICO
TR-90-4**

December 1990

*** PICO is operated by the University of Alaska Fairbanks under contract to the National Science Foundation, Division of Polar Programs.**

ABSTRACT

During the summer of 1989, PICO tested a prototype of a new deep ice core drilling system. The drilling system was designed for using diesel oil as drilling fluid. In the summer of 1990, the fluid was replaced with n-Butyl Acetate. Since n-Butyl Acetate is an extremely bad lubricant, the wear-rate on mechanical components was expected to be high.

The purpose of this study was to determine the wear on the motor and gear reducer in the drilling system and to evaluate potential situations for mechanical failures due to wear.

The motor and gear reducer were operated in an n-Butyl Acetate bath with a temperature between 0° and -10°C. Two failures occurred during the test, the first failure after 79 working hours and the second after 94 hours. Both failures were due to the same ball bearing breaking down.

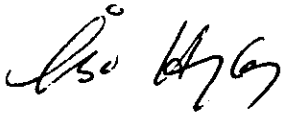
The lack of lubrication caused major problems. The endurance of the ball bearings was shortened noticeably. The wear-rate on other components in the gear reducer was high.

The lubrication mode in the motor and gear reducer could be improved by preventing the n-Butyl Acetate from surrounding the components. The motor and gear reducer could be placed inside a sealed container. The passage in the container for the output shaft could be sealed with Teflon seals, since n-Butyl Acetate does not dissolve Teflon.

PREFACE

The exchange program between the Luleå University and the University of Alaska Fairbanks provided the opportunity for us to complete our degree "Civilingenjör" in Mechanical Engineering (comparable to a Master of Science in Mechanical Engineering) in Fairbanks. We completed our degree with a final degree paper for Polar Ice Coring Office (PICO) at the University of Alaska Fairbanks.

Our paper was a study of wear on the motor and gear reducer system in a prototype deep ice coring drill. The study was a part of the evaluation of the drilling systems that was performed during the winter of 1990. The project at PICO introduced us to a (for us) new field of engineering applications, the very cold climate on the Greenland Ice Cap.



Åsa Hagberg

13 December 1990



Torbjörn Henriksson

ACKNOWLEDGMENTS

We do want to acknowledge Prof. Terry McFadden, School of Engineering, University of Alaska Fairbanks, and Dir. John Kelley, Polar Ice Coring Office (PICO), for all the support, both technical and editorial they have given us during this project. The Polar Ice Coring Office (PICO) is operated by the University of Alaska Fairbanks for the Division of Polar Programs, National Science Foundation. We also want to thank Prof. Erik Höglund, Department of Mechanical Engineering Höskolan i Luleå for helping us.

We want to thank Prof. Grant Baker and Eric Johansen at the School of Engineering, University of Alaska Fairbanks, for letting us use equipment and facilities within their departments at the University of Alaska.

Bruce Koci, Lori Smith and all the nice and friendly people at PICO should be given great credit for their interest, support and ideas, without which we couldn't have finished this project.

We also want to thank Linjenämnden Teknisk sektor at Höskolan i Luleå and the Swedish Civilingenjörers Förbundet for providing necessary economical support for us to go to Fairbanks, Alaska.

TABLE OF CONTENTS

1. Introduction	1
2. A Study Description	2
3. The Deep Ice Coring System	2
3.1. The deep ice core drill	3
3.2. The motor and reducer system	4
3.2.1. The motor	4
3.2.2. The gear reducer	5
3.3. The Drilling Fluid N-Butyl Acetate	6
4. An Approach to Wear	8
4.1. Wear-mechanisms	8
4.2. Different methods to measure and analyze wear	11
5. Experimental Methods	13
5.1. Measuring methods	14
5.1.1. Methods to measure working conditions	15
5.1.2. Methods to monitor wear	16
5.2. The Test Stand	16
6. Results	18
6.1. Working conditions for the motor and gear reducer	18
6.2. Wear on components in the circulate reducer	21
6.2.1. Contact between the circulate wheel and internal pins	25
6.2.2. Contact between the circulate wheel and bushings	29
6.2.3. Contact between bushings and carrier pins	31
6.2.4. Bearings	35
6.3. Wear on Components in the Motor	36
7. Conclusions and Recommendations	37
7.1. Possible solutions	39
8. References	40
Appendices:	
Appendix 1. The Motor and the Gear Reducer	42
Appendix 2. Monitoring Devices	48
Appendix 3. Construction of the Test Stand	53
Appendix 4. Changes in Working Conditions for the Motor and Gear Reducer System	58
Appendix 5. Changes in Rotation Speed When the Test System Broke Down ..	62
Appendix 6. Rotation Speed and Load in the Gear Reducer	63
Appendix 7. Contact Stresses on Components in the Gear Reducer	74

1. INTRODUCTION

The Polar Ice Coring Office (PICO) is operated under contract to the National Science Foundation (NSF) Division of Polar Programs by the University of Alaska Fairbanks, Fairbanks, Alaska, USA. One of PICO's responsibilities is to provide technical services, logistical support and field operations management to NSF-sponsored glaciological research programs. The Greenland Ice Sheet Program (GISP2) is a major project supported by NSF Division of Polar Programs. This project includes the development of a deep ice coring drill and the support system associated with it. The program objective of GISP2 is recovery of a high quality, continuous ice core through the Greenland Ice Cap (3,200 m). Analyses of the ice will provide a record of climate history covering 200,000 years or more .

To obtain a high quality core, the drill hole is filled with a fluid to maintain the pressure in the ice. Previously used fluids were various fuel oils with densifiers. These oils pose significant health, safety and environmental risks and can affect the chemical analyses of the ice core. An alternative fluid is n-Butyl Acetate, which does not affect the ice core nor the environment if leakage should occur. (1)

During the summer of 1989, PICO tested a prototype of a new deep ice coring system in Greenland. This drilling system was designed for using diesel oil as the drilling fluid. The following summer, the diesel fluid was replaced with n-Butyl Acetate. (2) From the experience of the last two summers drilling in Greenland, the new drilling system is operating effectively.

The effect of n-Butyl Acetate on the drill is not well understood. The internal components of the motor and gear reducer use the drilling fluid for lubrication. Since n-Butyl Acetate is an extremely poor lubricant, the wear-rate on mechanical components is supposed to be high. To improve the drill, it is important to know the rate and type of wear on the driving device. This report discusses a study of wear on the motor and gear reducer system as a result of operation in n-Butyl Acetate.

2. A STUDY DESCRIPTION

The first time that n-Butyl Acetate was used as the drilling fluid on the Greenland ice cap was in the drilling season the summer of 1990. The drill was operated for about 150 hours. Pieces of plastic and rubber were found in the ice slurry and the DC motor broke down after approximately 100 hours. The motor had to be replaced with a new one. The lifetime of every part of the drill should be higher than 150 hours so that the drilling work can be performed more efficiently.

To improve the drill, the design was evaluated during the winter 1990/91. Our part of the evaluation was to study how the motor and the gear reducer were affected by operating in n-Butyl Acetate. The purpose of our study was to:

- Determine the wear on the motor and reducer system as a result of operation in cold n-Butyl Acetate.
- Evaluate potential situations for mechanical failure due to wear.
- Evaluate causes for mechanical failure observed during the experiment

In order to test the motor and the gear reducer system during conditions which are as similar to drilling on Greenland as possible, the motor and reducer system were operated in an n-Butyl Acetate bath outdoors in Fairbanks, Alaska, during October-November. The temperature during this period was 0° to -10°C. The components were loaded by means of a brake and inspected for wear periodically.

3. THE DEEP ICE CORING SYSTEM

The depth of dry hole drilling in ice is limited to 200-300 m. Deeper dry holes usually give unsatisfactory core quality. The high content of compressed air in glacier ice cracks the ice if the pressure difference between the ice and the drill hole becomes too high. To drill deeper holes a densifier (usually a fluid) has to be added to

maintain the overburden pressure in the drill hole. Other advantages of fluid-filled holes are vibration damping and easy removal of ice chips from the drilling head. (2)

3.1. THE DEEP ICE CORE DRILL

The PICO drill developed for the Greenland ice cap is designed and built to produce high quality ice cores in fluid filled holes for the entire 3,200 m through the ice cap. This drill produces ice cores with a diameter of 13 cm and a length of 6 m. The hole in the ice has a diameter of 16 cm. A winch lifts the drill out of the hole to allow removal of the cores, one by one.

This drill is an expansion of PICO's 4 inch drill for dry holes. The construction is open, which means all parts of the drill are exposed to the drilling fluid. A schematic of the drill is shown in Figure 1. (3)

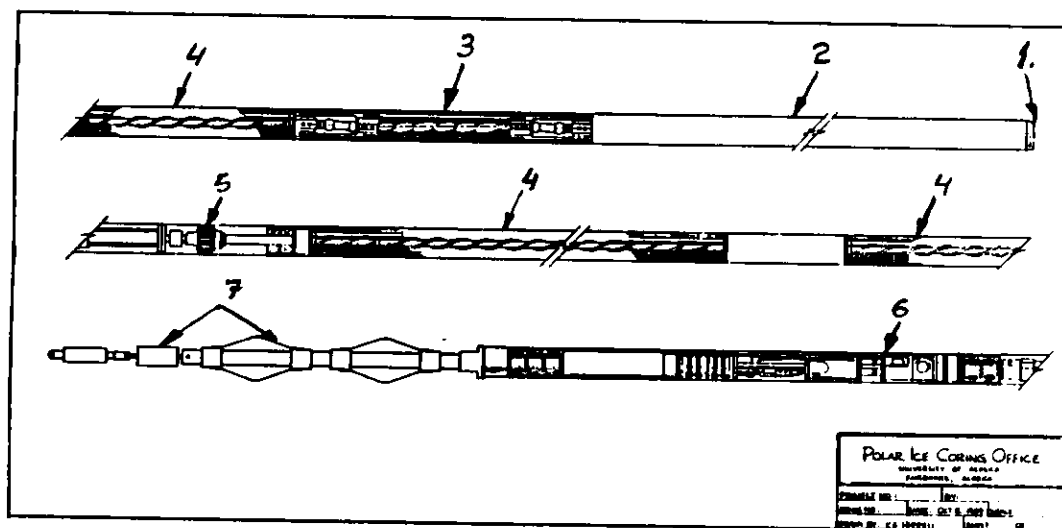


Figure 1. PICO deep ice core drill system.

1. Cutting head with core dogs (retainers)
2. Core barrel
3. Pump
4. Well screen
5. DC-motor and gear reducer system
6. Instrumentation and switch section
7. Anti-torque and slip ring

The ice chips are removed by the drilling head and transported along the outside of the core barrel by a feed screw. The slurry of ice and drilling fluid are pumped into the well screen by a Moyno, Inc., progressive cavity pump. Another feed screw pushes the slurry through the well screen, where the ice chips are removed from the fluid. The chips remain inside the screen and the fluid is recycled within the drill hole. The reason for this is to keep the hole free from ice chips. It is more difficult to pull the drill out from the hole if it is filled with ice chips than if the chips are removed.

When all parts are connected together they form a 22-29 m long cylinder with an outer diameter of 16 cm (equal to the hole diameter). The drill head has an operating speed between 60 and 200 RPM.

The anti-torque unit and the stabilizers will grip the ice in the sides of the hole and prevent the drill from rotating.

The instrument section contains various instruments for recording data which are required for good penetration control, for instance: penetration speed, depth, pressure and orientation. (3)

3.2. THE MOTOR AND GEAR REDUCER SYSTEM

The driving device of the drill contains an electric motor and a gear box connected together into one unit with coupling flanges (Figure 2).

3.2.1. The motor

The motor in the drill is a standard DC motor (Appendix 1). Various manufactures have been used. Some of the motors have run for a longer time, while others have broken down after only about 100 hours. There seem to be differences in how well motors from different manufacturers can work in liquids, specially in n-Butyl Acetate.

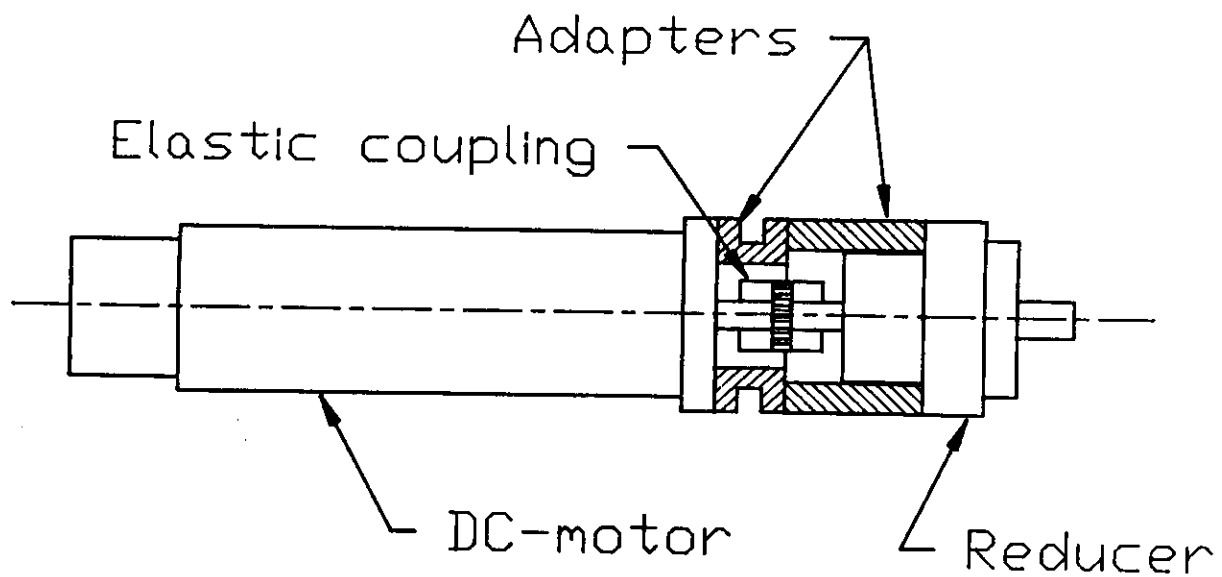


Figure 2. The motor and gear reducer system.

In this study a brush type DC motor from Honeywell was used. This motor produces 745.7 W at a speed of 1800 RPM. There is a tachometer (a DC generator) on the motor. This tachometer generates a DC voltage which is proportional to the speed (Appendix 2).

3.2.2. The gear reducer

A Graham Co., Inc., single circulate reducer, type 60 A 11 R, was used in this study. It is a gearless planetary gear box (Appendix 1). This reducer is not of the same size as the one that was used in Greenland during the summer of 1990. The reducer used in Greenland, type 60 B 17 R, is slightly bigger, but it operates in the same way.

3.3. THE DRILLING FLUID n-BUTYL ACETATE

When selecting an ice core drilling fluid, the density is of major importance. The fluid is added to the drill hole to maintain adequate pressure in the ice. The hydrostatic pressure is a function of density and depth. The drilling fluid's density must be higher than the density of the ice in order to obtain the necessary pressure. The density of n-Butyl Acetate increases rapidly with decreasing temperature. No densifier needs to be added when the mean temperature in the ice hole is lower than -20°C ; glacier ice is lighter than pure ice due to its high air content (Figure 3). (1)

A drilling fluid with low viscosity allows drilling of smaller holes. Higher viscosity demands larger diameter holes which require more time and energy. The viscosity of n-Butyl Acetate is about 1-3 cp (10^{-3} Ns/m^2) (Figure 4).

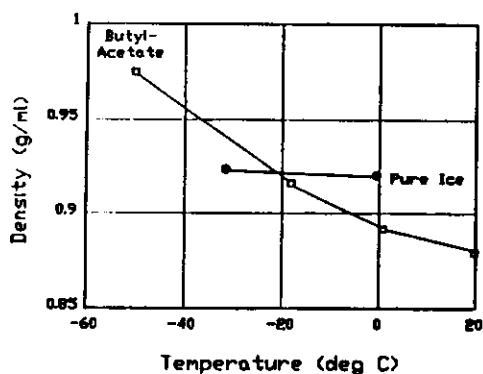


Figure 3. Density of pure ice and n-Butyl Acetate at different temperatures. (1)

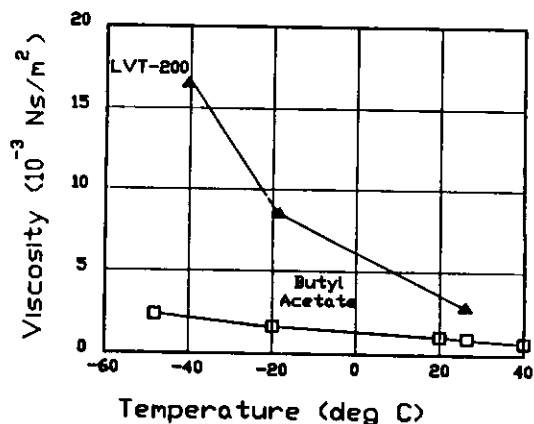


Figure 4. Viscosity of n-Butyl Acetate and another drilling fluid (LVT200 + PBBE) at different temperatures. (1)

n-Butyl Acetate (Figure 5) is a colorless liquid with a fruity odor that is detectable at 10 ppm. Some nasal irritation may be noticed at approximately 100 ppm, which still is well below the Occupational Health and Safety Administration's (OSHA) limit of 150 ppm. n-Butyl Acetate has an NFPA code of

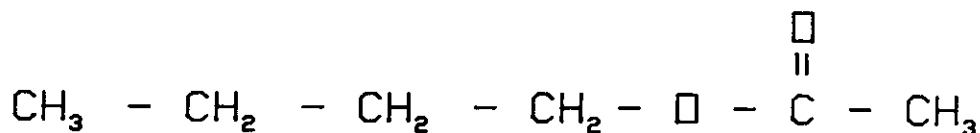


Figure 5. Chemical structure of n-Butyl Acetate

blue, which indicates that it is a compound which is slightly hazardous to health. n-Butyl Acetate has been shown to be slightly toxic to mammalian reproductive systems and is, at very high concentrations, slightly narcotic. The densifiers used with other drilling fluids (for instance PBBE), however, are suspected to be carcinogenic. (1)

If leakage should occur, n-Butyl Acetate will evaporate or biodegrade in a matter of days, even in a cold climate such as in Greenland. If all n-Butyl Acetate leaked out of the drill hole and flowed into a fjord, most would evaporate within three (3) days. A small amount would disperse into the water column and be rapidly biodegraded. (1)

Most polymer materials are affected by n-Butyl Acetate. Usually they swell and become softer. However, Teflon, some polyethylene and butyl rubber are not affected. (1) When the original seals, made of synthetic rubber, from the gear reducer were placed in an n-Butyl Acetate bath, the sealing edges deformed to a wave-shaped form after less than 12 hours and could not seal properly (Figure 6).

Grease from the reducer, placed in n-Butyl Acetate, was dissolved after a few hours. The lubrication mode in the gear reducer working in the drill is very poor since the viscosity of n-Butyl Acetate is so low and no chemical additives have been mixed with the drilling fluid to improve the lubrication properties. (4)

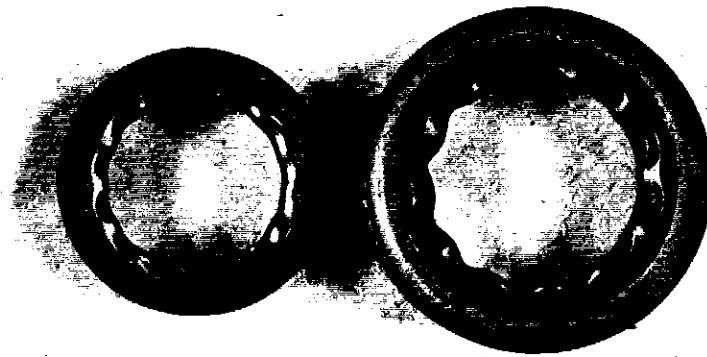


Figure 6. The sealing edge on seals after placed in a n-Butyl Acetate bath.

4. AN APPROACH TO WEAR

It is astonishing how limited our knowledge is about a problem as old as the machine. Wear is the undesired changes on the surfaces of useful articles by removal of small particles of material, due to mechanical or mechanical-chemical actions. The economic consequences of wear are of major concern since wear limits both the lifetime and the performance of machines with moving parts. The surface effects due to wear increase the possibilities for other types of damage, such as fatigue and stress corrosion. (5)

4.1. WEAR-MECHANISMS

There are many different mechanisms which cause wear. They are classified in many different ways. Usually the following categories of wear are recognized in

various classifications: adhesive and abrasive wear, surface fatigue and wear due to corrosion. (6,7)

Adhesive wear is the transferring of material from one surface to another, usually caused by asperities on one surface welding to those on the opposite surface. Adhesive wear can be divided into mild or severe wear, the latter is sometimes called *scuffing*.

Clean furrows cut by a hard particle or a protuberance on the surface are classified as *abrasive wear*. The responsible particle can be introduced from outside or produced by a chemical process on the surfaces. The type of *abrasive wear* which results when the particles are introduced by a surrounding liquid can be classified as *erosive wear*.

When pressure is applied on a surface, the maximum stresses appear below the surface. Cracks due to these stresses are finally propagated to the surface where pieces of the surface are detached. This phenomenon is often called *surface fatigue* or, if the cracks are parallel to the surface, *delamination*. (6,7)

Corrosion is caused by chemical attacks on the component's surfaces from the lubricant or the environment and can be promoted by electrical currents. Corrosion wear results either in removal of material or build up of deposits. The wear usually affects one phase in a two-phase material, such as steel. *Corrosion wear* can result in forming abrasive particles and supports fatigue. (8)

Vibrations and cyclic stresses can cause *fretting corrosion*. This type of wear appears when two loaded surfaces in contact undergo relative oscillatory tangential movements, "slips". When the two surfaces are made of steel the debris is usually a fine red powder. The debris can act as a lubricant and the slip zone will then become wider. Fretting corrosion can, as well as other wear mechanisms, initiate fatigue cracks. (7)

An attempt was made to unravel some of the confusion caused by all these different classifications by naming the wear mode *mild* or *severe* and relating the dominant wear mechanism to normalized data (Figure 7). (9,10) *Mild wear* gives a smooth surface and takes place under four different sets of conditions:

- Mild wear (i), when a thin elastic oxide layer between the asperities on the surface prevents metal-to-metal contact.
- Mild-oxidational wear (ii), when thicker and more brittle layers are continuously generated.
- At higher loads a hard surface layer is formed due to the higher flash temperatures and prevents metal-to-metal contact.(iii)
- The oxide layer deforms plastically due to high temperature and sliding velocity. The metal is partly insulated from the temperature, but the wear rate is high.(iv)

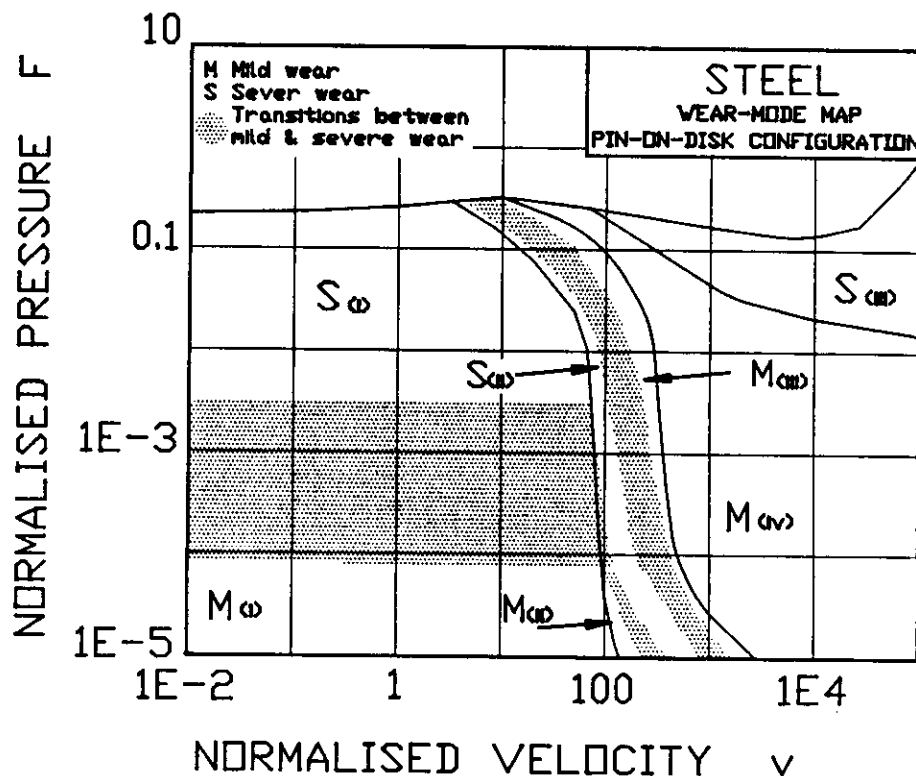


Figure 7. Wear mode map (9,10).

Severe wear gives a rough and deeply torn surface and the wear rate is usually higher. It takes place during these conditions:

- When the contact pressure during low velocities is high enough to rupture the oxide layer.(i)
- When the load is high enough to penetrate the thicker brittle oxide layer.(ii)
- If the sliding velocity is high enough to cause the flash temperatures to approach melting temperatures, melt wear. (iii)

The wear-mode map shows the mode of wear and the dominant wear mechanisms on a diagram with axes of normalized contact pressure and normalized sliding velocity. The map also shows the transitions between the different types of modes. There are three different types of transitions:

- The *load-dependent* transition from mild to severe wear, under increasing normal load, due to rupture of a thin oxide film on the surface.
- The *velocity-dependent* transition from severe to mild wear with increasing velocity due to the formation of hard martensitic surface layers, caused by the increasing flash temperature.
- The *distance-dependent* transition from severe to mild wear is often found during a running-in period of a sliding system and must be distinguished from the formerly described steady-state transitions.

4.2. DIFFERENT METHODS TO MEASURE AND ANALYZE WEAR

To increase our knowledge about how different parameters affect the wear rate, methods to measure the wear rate are of major importance. The material loss can quite accurately be measured as a change in weight, but this method does not describe the material damage or the redistribution of material. Precise surface maps,

produced by a profilometer before and after testing, describe the material damage, redistribution and the material loss. These maps are very informative, but expensive and time consuming to produce. A profilometer instrument can work in a range of very different ways: from a full map of the surface, complete with heights of points in a regular array, called a *mapping*, to one single profile of a cross section. (11)

There are a wide range of different methods to analyze wear and wear related failures. The similarity between the different methods is that each method is used as a checklist.

In "Wear control handbook" (6), a simplified system to characterize wear is described. The *wear-loss output* (Z) is defined as the result of the *operating variables* (X) and the *system's structure* (S) (Figure 8).

F.T.Barwell (7) describes a systematic way to present wear-related data by constructing a "profile" where the most important wear-related data are displayed (Figure 9). Further characteristics can be added to the profile if they are necessary for the analysis of the system exposed to wear. Sections two and three, Figure 9, show whether the system is conformal or nonconformal. Sections four, five and six together indicate the likelihood one of the surfaces may be overheated. The difficulty to obtain lubricated conditions is presented in section seven. Sections eight and nine describe the type of load. Hydrodynamic and geometric factors are represented in section ten.

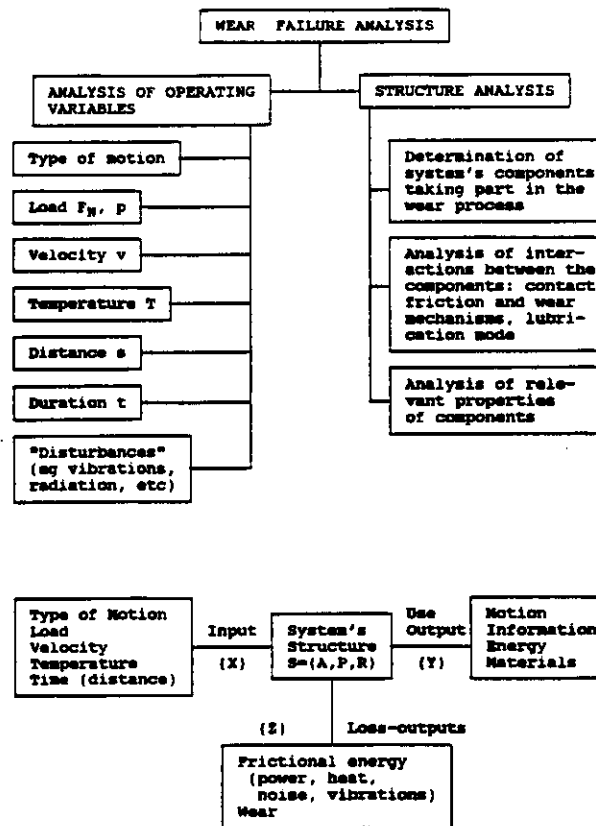
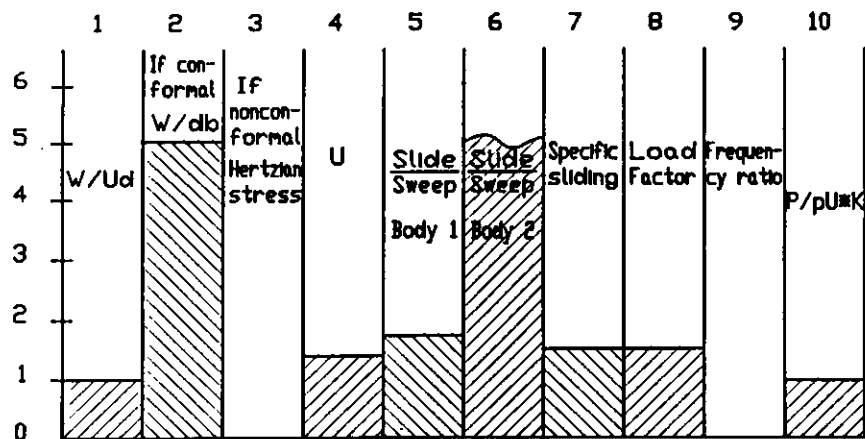


Figure 8. The wear-loss output as a result of the operating variables and the system's structure. (6)

5. EXPERIMENTAL METHODS

To simulate actual drilling conditions, the motor and reducer must be operated in a container filled with n-Butyl Acetate. The rotation speed of the drill head is 60 to 200 RPM and the electrical input power is about 400 W. To simulate the drilling force there has to be some type of load on the system, a generator or some sort of brake. The temperature in the drill hole is between 0°C and -57°C. To keep the experimental temperature as similar as possible to the temperature in the hole, the experiment has to take place outdoors during the winter or in a temperature-controlled room.



	Sliding velocity	Sweep velocity	Slide/sweep ratio	Specific sliding
	$u_1 + u_2$	u_1	$(1 + \frac{u_2}{u_1})$	$\frac{u_1 + u_2}{u_1 - u_2}$
	$u_1 + u_2$	u_2	$(1 + \frac{u_1}{u_2})$	
	$u_1 - u_2$	u_1	$(1 - \frac{u_2}{u_1})$	$\frac{u_1 - u_2}{u_1 + u_2}$
	$u_1 - u_2$	u_2	$(1 - \frac{u_1}{u_2})$	

Figure 9 A "profile" to display important wear-related data. (7)

5.1. MEASURING METHODS

The mechanisms of wear are closely related to the working conditions of the motor and gear reducer. To obtain a record of the working conditions during the experiment, several variables must be monitored.

To allow inspection for wear, the experiment has to be stopped about every 100 hours or when failure occurs. To assess the wear on the different surfaces of interest, the motor and the reducer must be disassembled.

5.1.1. Methods to measure working conditions

The optimal method when studying wear is to keep continual records of the working conditions. During this study the conditions were monitored about three times a day. The working conditions of major importance were:

- Temperature.
- Speed of rotation.
- Electrical input power and the load on the system.
- Environment. In this experiment the environment was the fluid n-Butyl Acetate in which the motor and the reducer were immersed all the time.

There are four different temperatures of interest: the temperature of the surrounding air, the n-Butyl Acetate bath and the temperatures of the motor and gear reducer. To measure these temperatures, type T thermocouples were used. A type T thermocouple is a junction of copper and constantan (an iron nickel alloy). The thermocouples were attached to a digital thermometer (Appendix 2). The thermocouples and the thermometer were calibrated before and after the experiments in an ice slurry, 0°C (32°F).

A DC tachometer on the motor was used to monitor the rotation speed of the motor. The rotation of the output shaft of the reducer is 11 times slower than the motor rotation. The voltage from the tachometer was continually monitored by a strip chart recorder. To calibrate the tachometer voltage, the rotation was also measured with a hand tachometer to create a calibration curve from voltage to revolutions per minute (Appendix 2).

The electrical input power was measured by a voltmeter and an ammeter in a direct current converter. The system was loaded with a motorcycle disc brake and the torque was monitored with strain gages bonded on the brake shaft. The gages formed

a Whitestone bridge on the shaft and were attached to a strain indicator via a slip ring. The strain indicator was calibrated by applying a torque using weights and a lever to obtain the correlation between the load (Nm) and the reading from the strain indicator (μ strain) (Appendix 2).

5.1.2. Methods to monitor wear

The components suspected to have the highest wear were, when possible, weighed and their dimensions were measured with a micrometer (Appendix 2). In the reducer, the bushings and the circulate wheel were both weighed and measured. The carrier pins and the brushes in the motor were also measured with a micrometer and caliper respectively.

The surfaces of interest on the components were studied by microscopes in order to determine the wear mechanisms. Some of those surfaces were photographed for documentation.

To estimate the wear rate, samples from the n-Butyl Acetate bath were sent for spectrometry analysis to Spectro Analytic Inc., Dallas. An increase in a particular element in the bath indicates which components have the highest wear rate because of different alloys in the components. The various materials of the components in the motor and reducer indicate the metals of major interest. They were iron (Fe), copper (Cu), chrome (Cr), molybdenum (Mo) and manganese (Mn) (Appendix 1).

5.2. THE TEST STAND

The motor and the gear reducer were placed in a bath of n-Butyl Acetate. To contain the fluid, a trough 3 feet long and open at both ends was manufactured. The trough and end pieces can be attached to PICO's other equipment for testing drilling

systems. An end piece is bolted in each end of the trough and the connections are sealed with cork gaskets. Cork is not affected by n-Butyl Acetate (Figure 10).

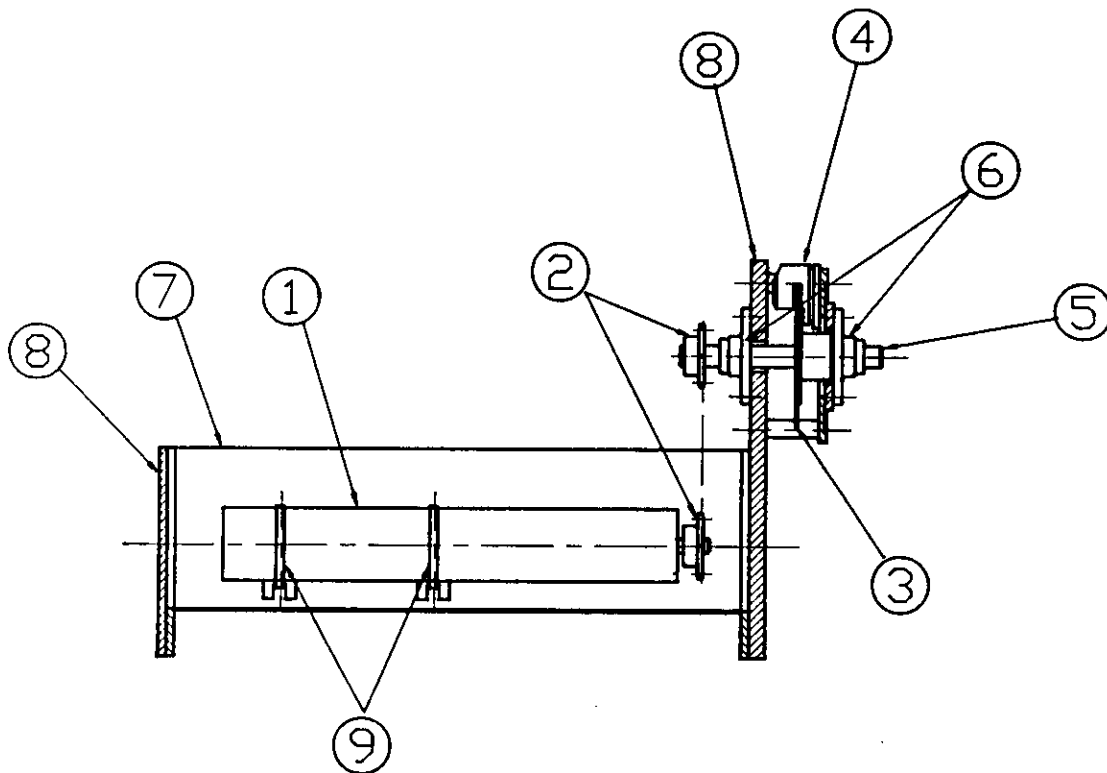


Figure 10. Test stand of the motor/gear reducer system.

1. Motor and gearbox
2. Sprockets and chain
3. Disc brake
4. Brake blocks
5. Brake shaft
6. Ball bearings
7. Test chamber (trough)
8. End pieces
9. Hose clamps

A disc brake from a motorcycle was used to load the system. The brake cannot operate in n-Butyl Acetate, so it has to be located out of the fluid. It is easier to place the brake above the bath and use a transmission drive between the reducer and the brake than to seal a chamber inside the fluid. In this case a chain drive was selected. A V-belt, for instance, cannot operate in n-Butyl Acetate (Appendix 3).

To create a constant load, the pressure on the brake pads must be constant. Two different methods were used to obtain the required constant pressure. The first 79 hours, a brake handle from a motorcycle was connected to the disc brake and loaded by a spring. Leakage caused the pressure on the brake pads to drop notably over a couple of hours. During the last 15 hours, compressed air via a pressure regulator kept a constant pressure on the brake oil and therefore the loaded torque was kept uniform. The shaft through the brake was supported by two ball bearings (Appendix 3).

To prevent the motor/reducer system from rotating, four supports were welded to the bottom of the trough. The system was attached to the trough with two hose clamps through holes in the supports.

To protect the rotating parts, covers were made to be placed over the chain and over the brake. Another cover prevented the n-Butyl Acetate from evaporating.

6. RESULTS

The experiment ran from 20 October to 3 November 1990. Two failures occurred during the experiment, the first failure after 79 hours and the second after 94 hours. Both failures were due to breakdown of the small ball bearing on the input shaft of the gear reducer. The ball bearing was replaced after the first failure with a new bearing so that the experiment could continue.

6.1. WORKING CONDITIONS FOR THE MOTOR AND GEAR REDUCER

Unfortunately, the load on the motor-reducer system was not constant during the first experimental period, 0-79h. The variation in load caused a variation in both the rotational speed and the electrical input power to the system. The load varied between 4.1 and 39.9 Nm, the input power between 124 and 564 W and the

rotation speed on the input shaft of the gear reducer varied between 824 and 1236 RPM.

During the second period, 79-94h, the load varied between 28 and 32 Nm, when the new brake system had been adjusted. The variables are displayed in Appendix 4.

The outdoor temperature variations and the corresponding temperatures in the motor and reducer during the experimental periods are displayed in Figure 10. The outdoor temperature varied between -13.5°C and -2.7°C (Figure 11).

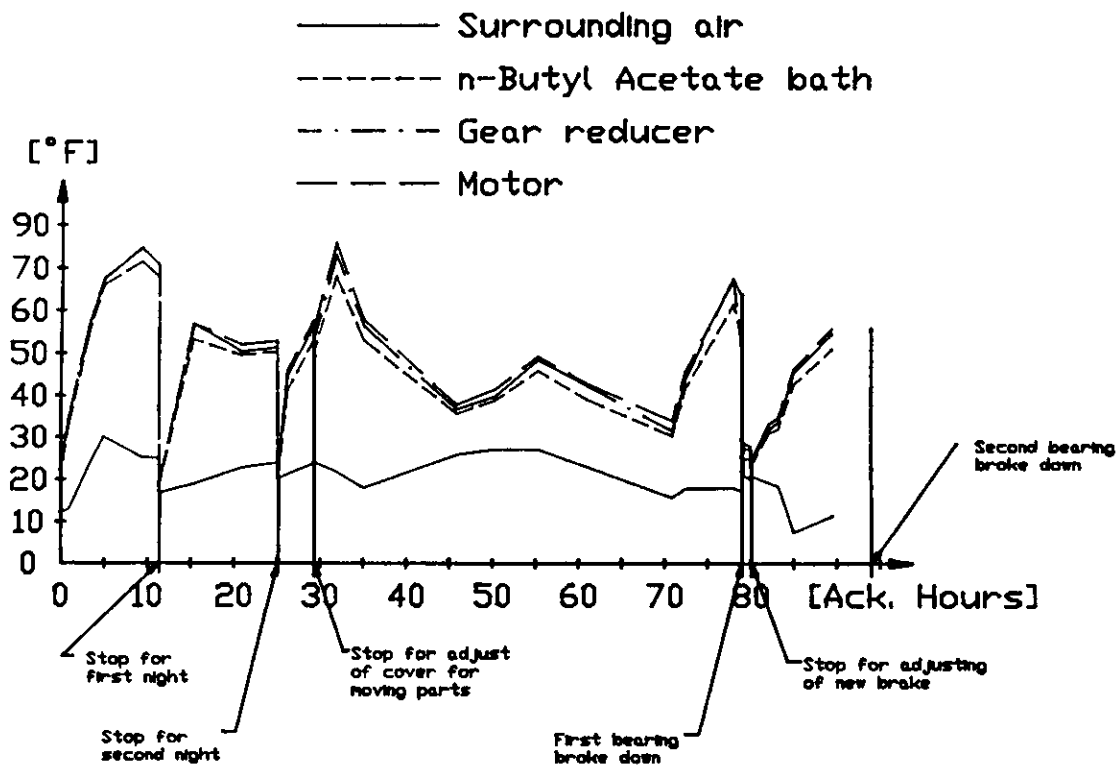


Figure 11. The temperatures during the experimental periods.

The first failure occurred after 79 hours when the small ball bearing on the input shaft of the reducer failed, freezing the shaft (Appendix 5). The temperature in the reducer had increased to 17.5°C , and was higher than the temperature in the motor (11°C). The input power to the motor rose to 2075 W. When the bearing failed,

three of the seven balls were parted into at least two pieces (Figure 12). One half of a ball ended up between one bushing (#3) and the corresponding hole in the wheel. The bushing was broken into two parts (Figure 13).

The bearing was replaced with a new bearing for the second experimental period. After an additional 15 hours (total 94h), the new ball bearing failed. Unfortunately, this failure occurred in the middle of the night so there is no record of the temperature just before the failure. The motor was still trying to run the reducer and that caused the temperature in the bath to rise to about 125°C, the boiling temperature for n-Butyl Acetate. The polyethylene cover on the cables melted and after 1 hour 27 min the motor stopped due to the destroyed cables (Figure 14). Every ball in the bearing was broken and pieces were scattered throughout the reducer (Figure 15).

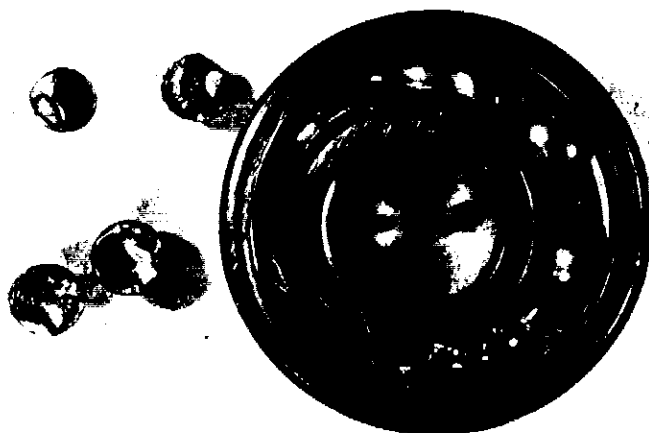


Figure 12. The first ball bearing failed after 79h.



Figure 13. The bushing parted when the bearing failed, 79h.

The endurance for two ball bearings of the same type can vary a lot. The large difference in endurance in this study could be reinforced by the use of a constant load during the second period instead of a periodical load.

6.2. WEAR ON COMPONENTS IN THE CIRCULUTE REDUCER

The most interesting components, with respect to wear, in the reducer are the power transmitting components: the circulate wheel, internal pins, bushings and carrier pins, and the two ball bearings on the input shaft. Since rotation speed is much higher on the input shaft than on the output shaft, the bearings on the input shaft are more interesting than the ball bearings on the output shaft. The wear components are described in Appendix 1 and shown in Figure 16. The velocities of the components and the forces acting on them are estimated in Appendix 6.

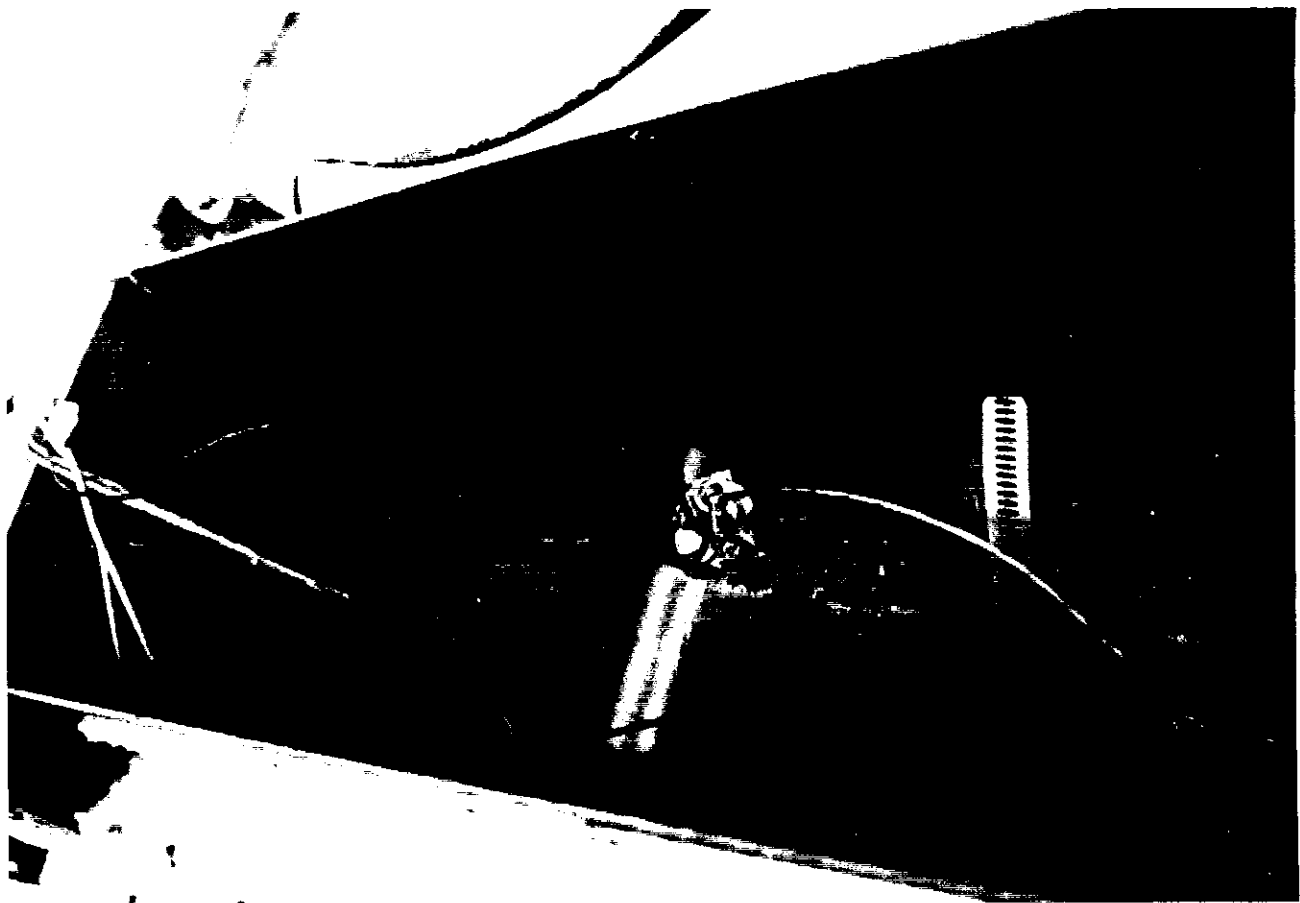


Figure 14. The temperature in the n-Butyl Acetate bath rose to about 125°C and the polyethylene cover melted.

The components were completely surrounded by n-Butyl Acetate. Since this fluid is an extremely poor lubricant, the surfaces were actually in contact with each other with no protecting lubricant film between them.

When the ball bearings failed, small pieces from the bearings were scattered around in the reducer. Some pieces from the bearings found their way into the contact zones and ploughed furrows on the surfaces. This type of abrasive wear was detected on several of the examined surfaces.

The presence of wear on the bushings and circulate wheel could be detected by weighing them. The differences in weight during the experiment were small, but they clearly indicated a trend of decreasing weight (Table 6.1).

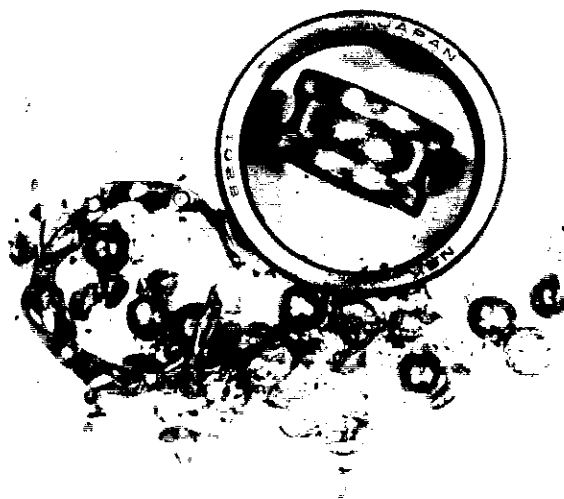


Figure 15. The second ball bearing failed after 15h.

The weight of the circulate wheel followed the same trend. The weight decreased from 160.04 g in the beginning, to 159.92 g after 79 hours and 159.89 g after 94 hours.

The spectrometry analyses showed an increased ratio of the most interesting elements (Table 6.2). The ratio of iron increased from 5.0 to 28.0 ppm (detection limit 0.05 ppm) during the first 79 hours. The ratio of molybdenum has probably increased, but the detection limit is significantly higher than for the other elements. The bottle containing the 94 hours sample broke and some of the sludge at the bottom may have been lost. The color of the 94h sample was darker than the 79h sample and

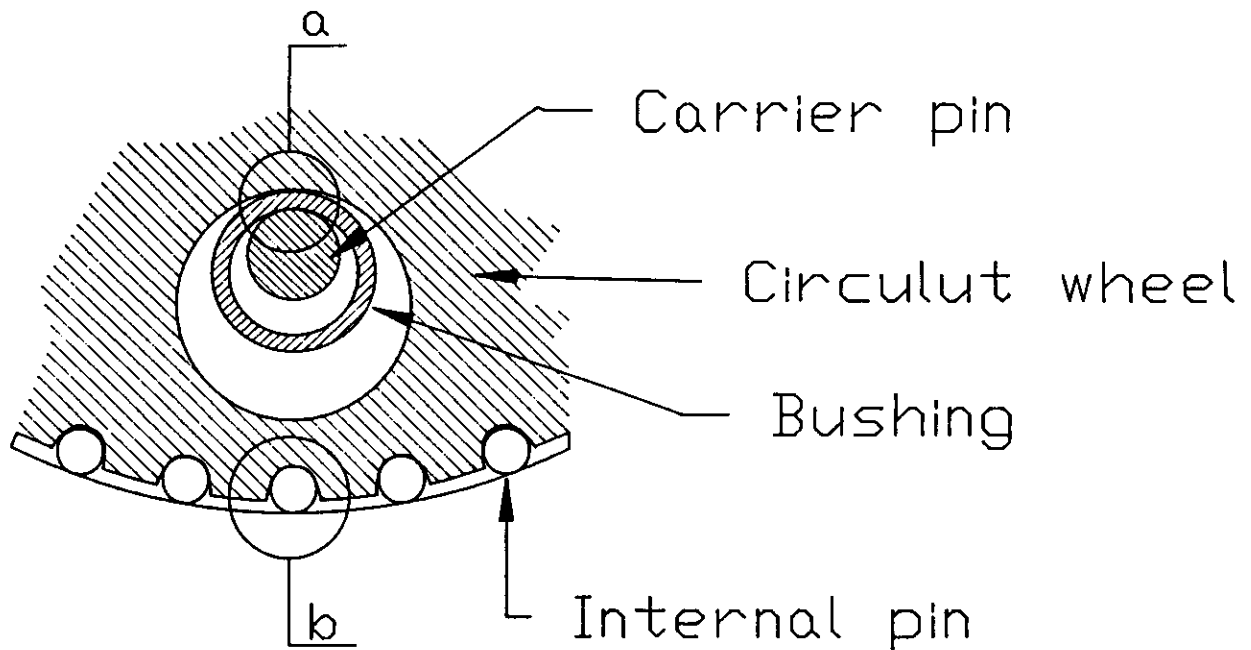


Figure 16. a) The contact between the circulate wheel, bushings and carrier pins.
b) The contact between the teeth of the wheel and the internal pins.

Table 6.1. Weights of bushings (grams).

Hours of Operation	BUSHING #							
	1	2	3	4	5	6	7	8
0	2.68	2.68	2.70	2.68	2.69	2.69	2.70	2.69
79	2.68	2.67	—	2.67	2.67	2.68	2.69	2.67
94	2.67	2.67	—	2.66	2.67	2.67	2.69	2.67

Table 6.2. Ratio of different elements (parts per million) in the n-Butyl Acetate bath after 0, 79 and 94 hours.

Element in the sample	Ratio (ppm) after X hours			Detection limit (ppm)
	0	79	94	
Chromium	N/D	0.93	1.11	0.10
Copper	0.30	3.50	2.92	0.05
Iron	5.00	28.0	21.1	0.05
Manganese	N/D	0.30	0.27	0.05
Molybdenum	N/D	N/D	N/D	0.50

Spectro-Analytic, Inc., who analyzed the samples, suspected the ratio of different elements to be higher.

6.2.1. Contact between the circulate wheel and internal pins

The force normally applied to the contact between the teeth of the circulate wheel and the internal pins is about 211 N and the relative sliding velocity is about 0.19 m/s (Appendix 6). Approximate values of the contact area and the stresses in the contact center are estimated in Appendix 7. The contact area is about 0.7 mm². The stresses on the surfaces are:

$$\sigma_{yy} = -220 \text{ MPa} \quad \sigma_{xx} = -367 \text{ MPa} \quad \sigma_{zz} = -367 \text{ MPa} \quad \tau = 0$$

The maximum shearing stress and the corresponding principal stresses appear at a depth of 60 μm below the surface and are estimated at:

$$\sigma_{yy} = -107 \text{ MPa} \quad \sigma_{xx} = -68 \text{ MPa} \quad \sigma_{zz} = -288 \text{ MPa} \quad \tau_{\max} = 110 \text{ MPa}$$

In the beginning, the internal pins were bonded to the housing of the gear reducer. When the bond was dissolved by the n-Butyl Acetate, the pins became loose and could rotate. The rotation can slightly affect the efficiency of the reducer but is not supposed to cause major problems. The pins are retained in the right places since they are placed in small holes in the housing. When the first bearing failed after 79 hours, the circulate wheel climbed out of position and disengaged from the pins. The wheel deformed areas on the surfaces of about eight pins. The deformed zone from the first bearing failure and the wear due to the rotation of the pins are visible in Figure 17. After 94 hours, the surface of the contact zone on the pins was deformed plastically to a smoother surface with no machining marks visible (Figure 18).

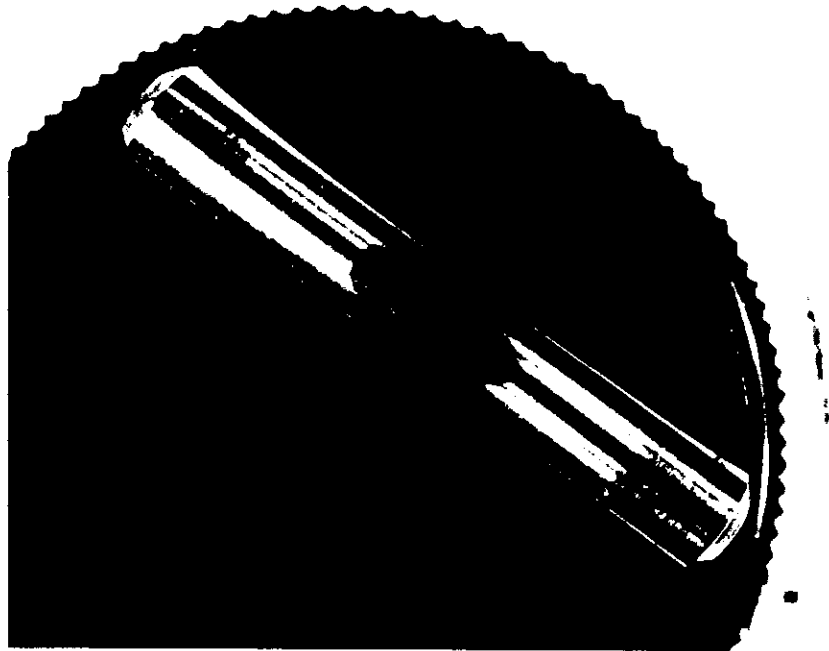


Figure 17. An internal pin; the deformed zone from the first bearing failure is visible in the middle and the rotation marks appear to the right.

The teeth on the circulate wheel have been deformed. The back edge of the tooth material hangs over the edge while the front edge has become more rounded (Figure 19 and 20). When a pin comes into engagement, it slides over the top of the tooth and deforms the back edge of the tooth. On some teeth small pieces of material

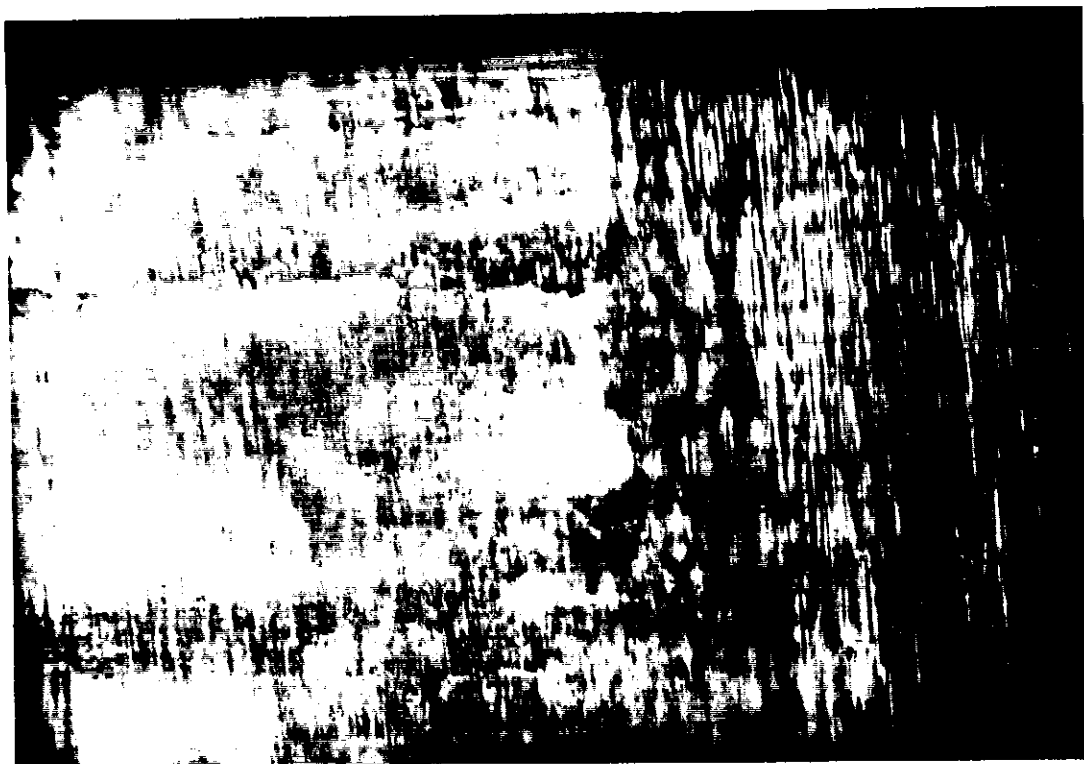


Figure 18. The plastically deformed surface (to the left) in the contact zone between the internal pin and the circulate wheel (94h).

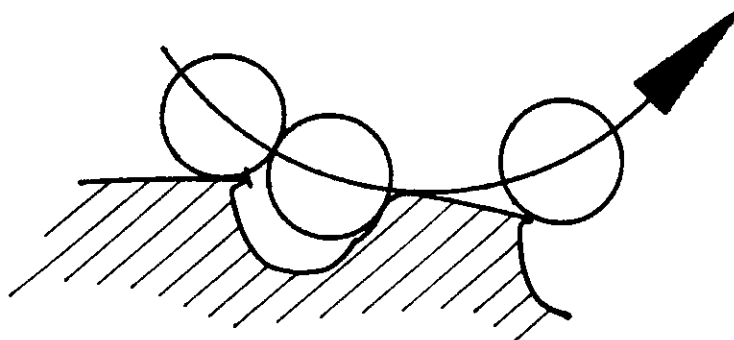


Figure 19. Sketch of the relative motion between the wheel and pins and the type of deformation on the teeth of the wheel.

are missing from the back edge (Figure 21). The front parts of the teeth have slightly deformed surfaces where the wheel is in contact with the pin while rotating round it. The contact stresses approach the elastic limit (Appendix 1) and some of the deformations might have been plastic. The wear rate is high and the damage on the teeth can cause major problems if allowed to continue. The damage of the tooth shape

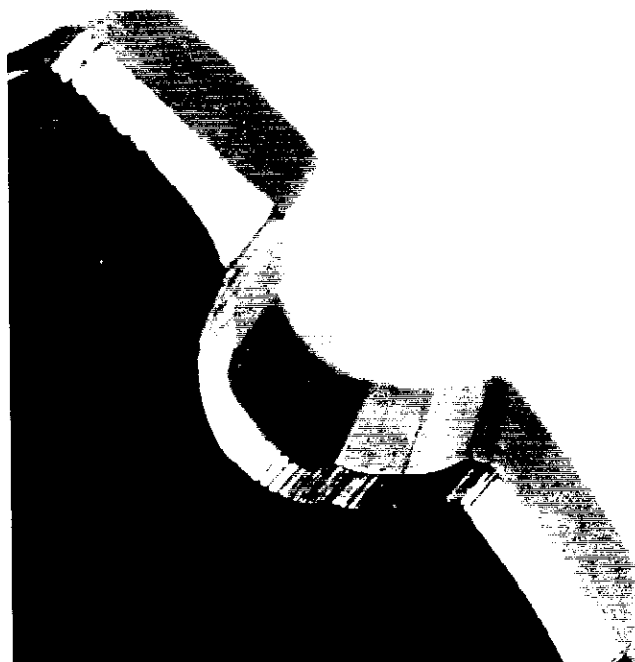


Figure 20. The front edge of a tooth of the wheel after 94h.

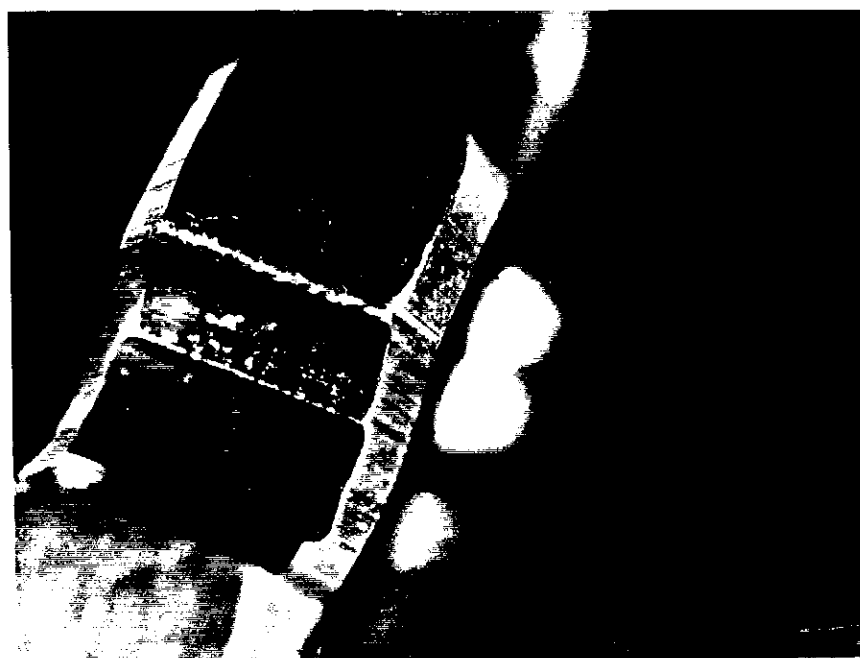


Figure 21. The back edge of a tooth of the circulate wheel after 79h.

can lower the efficiency of the reducer. When the damage is substantial, the wheel can miss some of the pins and generate an uneven output rotation. The damage can also cause break down.

6.2.2. Contact between the circulate wheel and bushings

The force normally applied to the contact between the circulate wheel and the bushings is about 343 N (Appendix 6). The contact area is estimated to be about 1.3 mm² (Appendix 7). The contact stresses are also estimated in Appendix 7. The stresses on the surface are approximately:

$$\sigma_{yy} = -201 \text{ MPa} \quad \sigma_{xx} = -335 \text{ MPa} \quad \sigma_{zz} = -335 \text{ MPa} \quad \tau = 0$$

The maximum shearing stress appears 107 μm below the surface. The shearing stress and the corresponding principal stresses are estimated to be:

$$\sigma_{yy} = -98 \text{ MPa} \quad \sigma_{xx} = -62 \text{ MPa} \quad \sigma_{zz} = -263 \text{ MPa} \quad \tau_{\max} = 101 \text{ MPa}$$

The relative motion between the wheel and carrier pins varies between 2.3 and 7.7 m/s. The relative velocity depends on where the carrier pin is located compared to the internal pins in contact with the circulate wheel (Appendix 6). The bushing slides between the surfaces of the wheel and the carrier pin. The relative velocity between the wheel and bushings is probably about half of the velocity of the carrier pins relative to the wheel. The velocity might be slightly lower due to a larger surface in contact with the wheel than with the carrier pins. The relative sliding velocity between the wheel and the bushings should be about 1.1-3.8 m/s.

The machining marks are still visible on the surfaces inside the holes of the circulate wheel. The surfaces of the loaded zones inside the holes are however

polished. The surfaces are smooth with a reddish tone and no machining marks can be detected in these zones (Figure 22). The borders between the unloaded and loaded



Figure 22. The polished zone inside the holes of the circulate wheel after 79h.

zones are very distinct. The locations of the loaded zones are explained in Appendix 6 and shown in Figure 23.

After 79 hours, the manufacturing marks are still visible on the outer surfaces of the bushings, but a band around the bushings is polished and has a reddish tone (Figure 24). After 94 hours, small marks have been developed in the polished zone. The marks seem to be due to the bushings sliding motion relative to the wheel and they resemble brush marks on an oil painting (Figure 25).

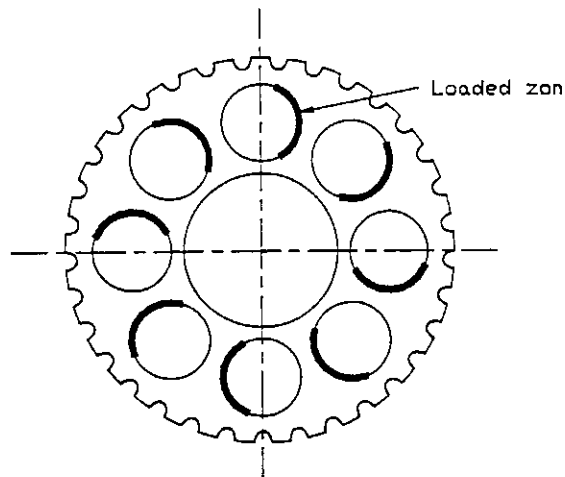


Figure 23. The location of the loaded zones of the holes in the circulate wheel.

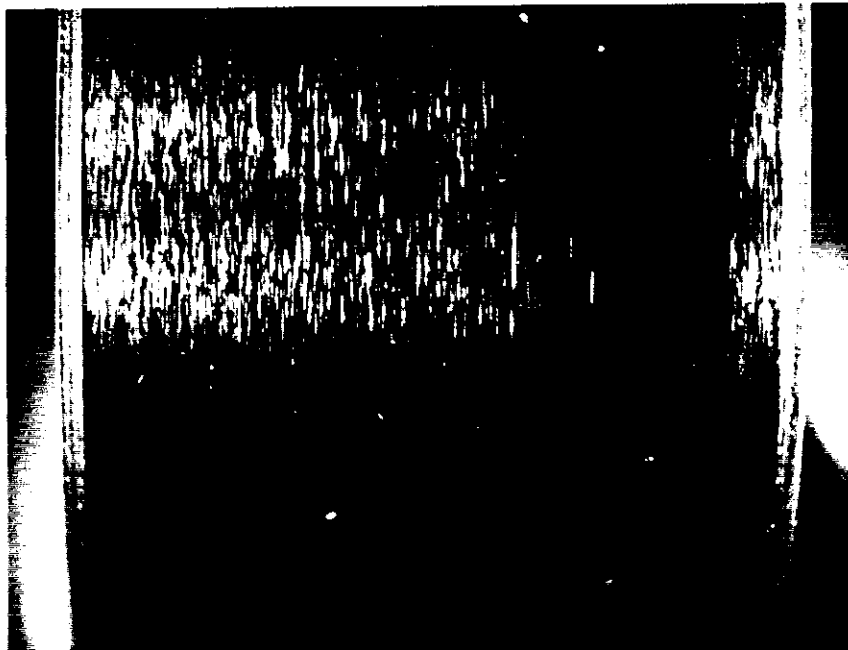


Figure 24. The polished band on the surfaces of the bushings after 94h.

6.2.3. Contact between the bushings and carrier pins

The force normally applied to the contact between the bushing and the carrier pin is also 343 N. The relative sliding velocity between the carrier pins and the bushings probably varies between 1.2 and 4 m/s. In Appendix 7, the contact area is

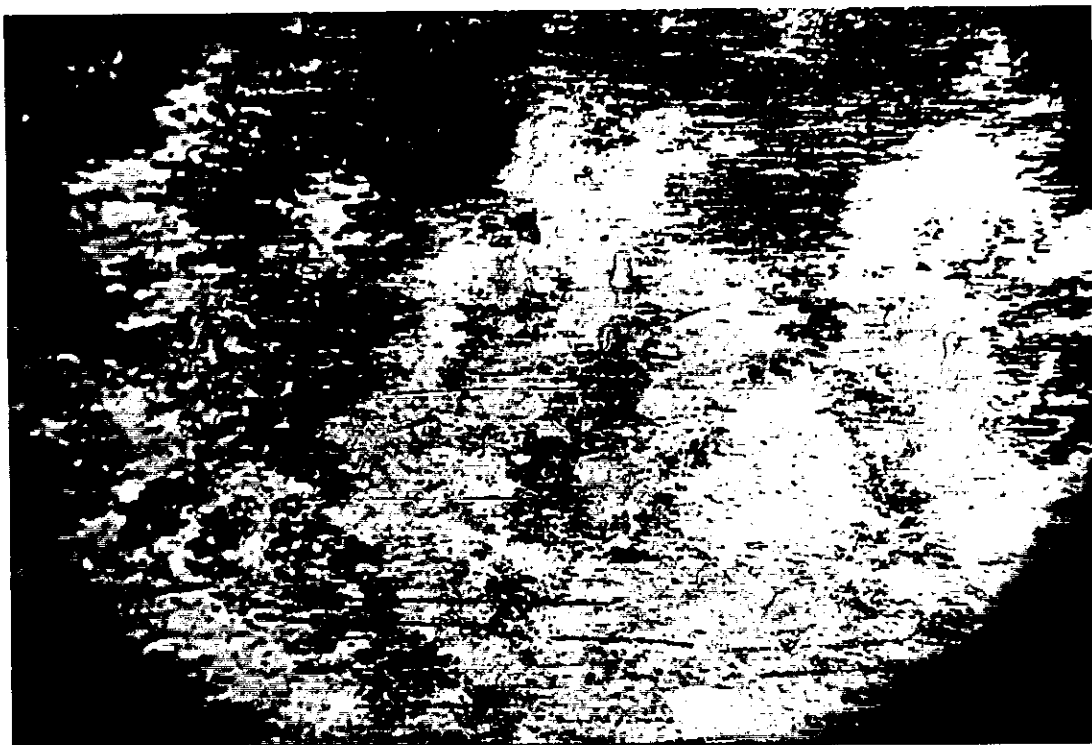


Figure 25. The sliding marks on the polished surface of the bushing after 94h.

estimated to be about 1.0 mm^2 and the corresponding stresses on the surface in the contact center are:

$$\sigma_{yy} = -260 \text{ MPa} \quad \sigma_{xx} = -433 \text{ MPa} \quad \sigma_{zz} = -433 \text{ MPa} \quad \tau = 0$$

The maximum shearing stress appears at about $83 \text{ }\mu\text{m}$ below the surface in the center of the contact. The maximum shearing stress and the corresponding principal stresses are estimated to be:

$$\sigma_{yy} = -126 \text{ MPa} \quad \sigma_{xx} = -80 \text{ MPa} \quad \sigma_{zz} = -340 \text{ MPa} \quad \tau_{\max} = 130 \text{ MPa}$$

The loaded zones on the carrier pins are polished to smooth reddish surfaces, while the machining marks are still visible in the unloaded zones. The loaded zones

of the carrier pins are located correspondingly to the loaded zones of the circulate wheel (Figure 26). The shape of the carrier pins is slightly deformed. After 94 hours the original round shape is flattened in the loaded zone (Figure 27). The contact stresses are higher than the approximate elastic limit, 280 MPa, and some of the deformation could be plastic while some deformation probably is due to removal of

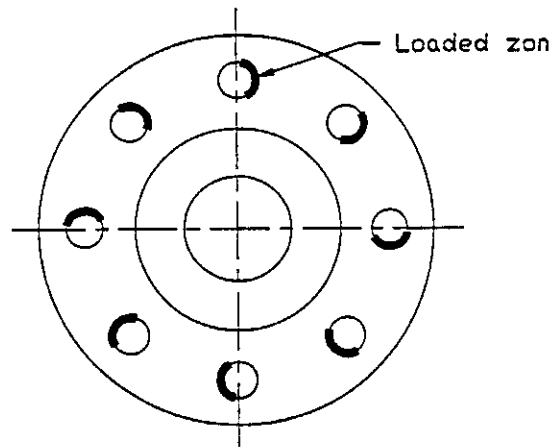


Figure 26. The location of the loaded zones on the carrier pins.



Figure 27. The loaded zones of the carrier pins after 94h.

material from the surfaces. The major problem with this type of damage is the increased possibility for fatigue failure.

After 79 hours, the inner surfaces of the bushings are reddish with brighter stripes at approximately a right angle to the slip motion (Figure 28). After 15 more

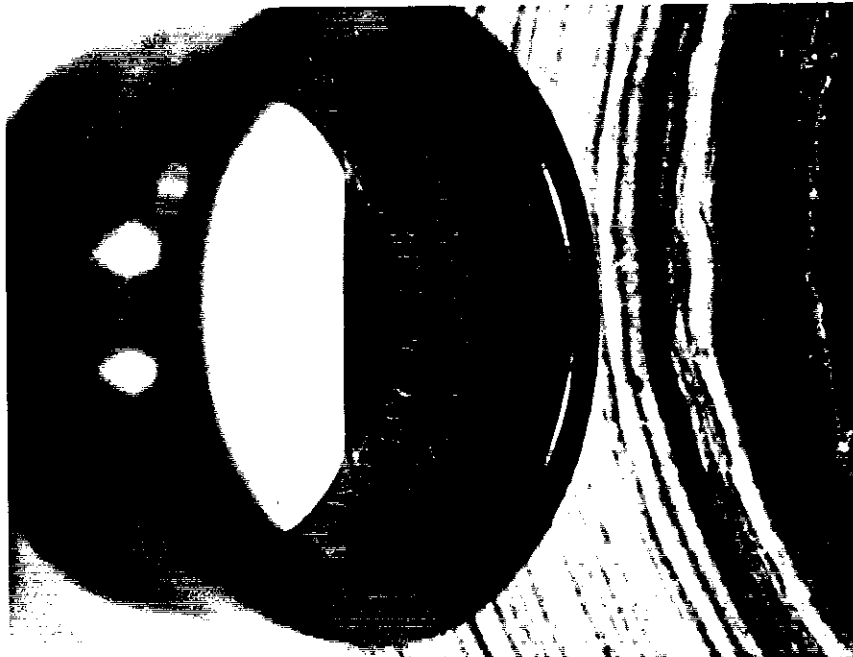


Figure 28. The brighter stripes on the reddish inner surface of the bushing after 79h.

hours, the stripes are much wider and cover more of the surface (Figure 29). The most visible stripes are located on the same side of the bushing as the polished band described above. This is the side of the bushing closest to the connection between the carrier pin and the output shaft. A small elastic deformation of the carrier pins probably reduces the contact stresses on the end of the pin which is farthest from the output shaft.

The higher contact stresses and the higher sliding velocity, compared to the contact between the wheel and the bushing, indicate a higher wear rate.

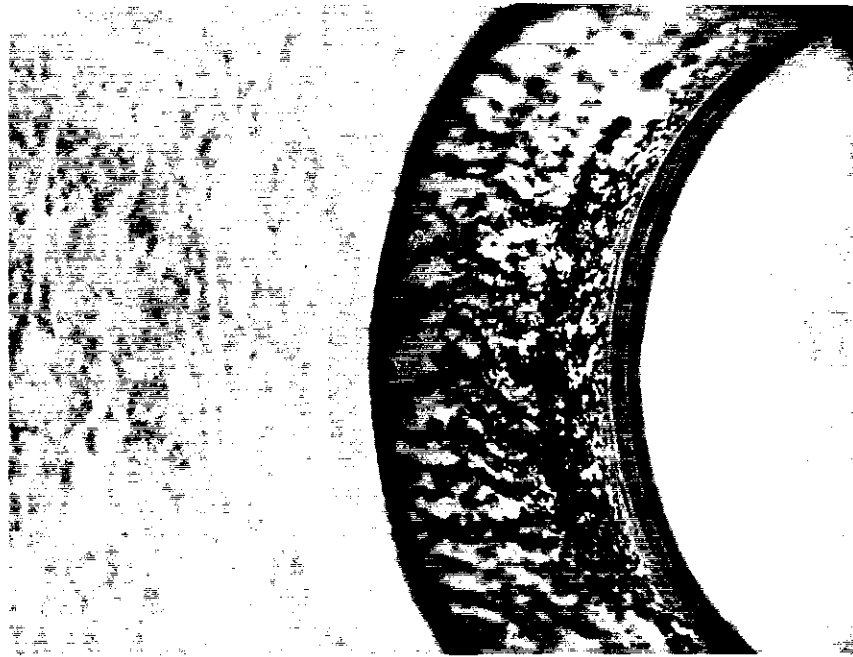


Figure 29. The inner surface of the bushings after 94h.

6.2.4. Bearings

The two small ball bearings on the input shaft that failed (bearing₂ in Appendix 1) broke down after 79h and 15h. The balls were broken and crushed. The relative velocity between the inner and outer ring in the bearing is about 102.83 rad/s and the load on it 444 N (Appendix 6).

The typical fatigue pattern, which looks like waves in beach sand, was not visible on the failure surfaces of the balls. The surfaces had differences in height and resembled brittle fractures (Figure 30). There were no marks or discoloration that indicated that the failure was due to high temperature in the ball bearing.

On the small bearings' outer races, a pattern of "dots" was found. This might be a sign of fatigue on the race surfaces and might have caused the failure.

The relative velocity between the outer and inner ring on the larger ball bearing on the input shaft (bearing₁ in Appendix 1) is about 94.25 rad/s. The load on

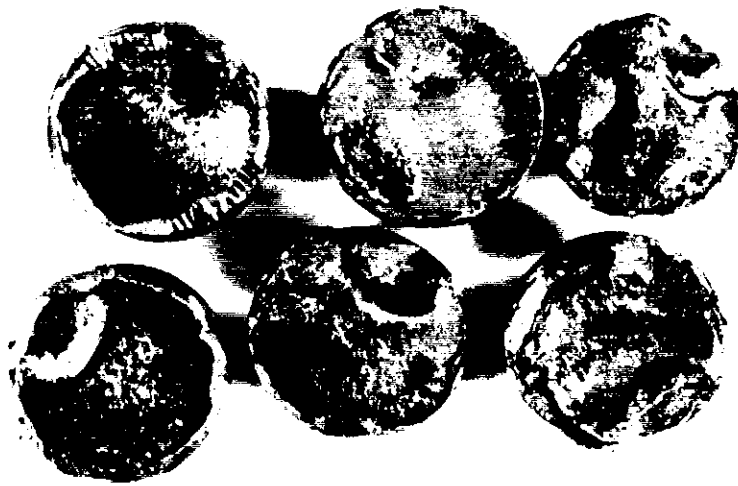


Figure 30. The fracture surface of the balls from the first ball bearing, 79h.

this ball bearing is about 331 N (Appendix 6). The ball bearing was still working after 94 hours, but generated more noise than in the beginning. After 79 hours, the noise stopped when the bearing was lubricated with a small amount of oil. After 94 hours the noise did not stop when the bearing was lubricated.

The large bearing's outer race had the same pattern as the small ball bearings' outer races (Figure 31). The pattern resembles photos of surface fatigue in "Tribology: friction, lubrication and wear" (6).

On the inner race of the larger ball bearing, furrows in the rotation direction were visible. The possible fatigue pattern was detectable (Figure 32).

6.3. WEAR ON COMPONENTS IN THE MOTOR

The wear rate in the motor seems to be smaller than the wear rate in the reducer. The ratio of copper in the bath increased significantly during the first



Figure 31. The pattern of "dots" on the larger ball bearing's outer race, 94h.

79 hours. The components suspected to have a high content of copper are the brushes, the winding and the brush-rocker. No decrease in the length of the brushes could be detected, and the copper winding looks fine.

There is no noise from the ball bearings in the motor. The motor worked well again when the destroyed cables (due to the second bearing failure) had been replaced with new ones.

7. CONCLUSIONS AND RECOMMENDATIONS

The working conditions for the motor and reducer system were slightly different in this study than the conditions in a drilling system in the field.

The temperature of the surrounding fluid was too high. The average temperature in the fluid is about -20°C when drilling on Greenland and the average



Figure 32. The furrows and the fatigue pattern on the inner race of the larger ball bearing after 79h.

temperature during this study was about 6°C. The difference in viscosity for n-Butyl Acetate due to this temperature difference is small so the temperature has not changed the conditions significantly.

Due to the problems with the brake, the load on the test system was lower in this study than the load on the field system during an actual drilling operation. The test system operated continually and not periodically, like the real drilling system.

The surrounding fluid was the same as the drilling fluid. When the drill is hoisted up from the drill hole, the fluid is drained out of the motor and gear reducer, so the field system is exposed to air periodically.

There was no grease left in the reducer that had been working in the field drilling system. The removal of grease from the reducer in this study created lubrication conditions similar to the conditions in the field drilling system. During

this study no pieces of rubber were found in the fluid, which might have been the cause of the motor break down in the field drill.

The reducer in the drill is slightly bigger than the reducer used in this experiment. The larger reducer has a roller bearing instead of the ball bearing which failed. A roller bearing is tougher than a ball bearing and was probably the difference between the two systems. The larger ball bearing on the input shaft of the test system is the same type of bearing used in the field system. Other ball bearings in the reducer from the field drilling system are equal to their counterparts in the test reducer. After about 150 hours of drilling, the ball bearings in the reducer from the drilling system also created noises when they were rotated.

The lack of lubrication caused major problems. The endurance of the ball bearings was shortened noticeably when they were working in n-Butyl Acetate. The wear rate on other components in the gear reducer was high. The ratio of chrome in the surrounding fluid increased from "not detectable" (less than 0.10 ppm) to 0.93 ppm in 79 hours. The materials in the bearings, internal pins, circulate wheel, bushings and carrier pins are chromium alloyed steels.

Failures of the gear reducer are most likely to be due to the shortened endurance of the ball bearings. The damage on the teeth of the circulate wheel and the increased possibility for fatigue failures may also cause a shortened endurance for the motor and gear reducer system.

7.1. POSSIBLE SOLUTIONS

To increase the endurance of the ball bearings, better lubrication modes can be created. There are solid lubricants that are not dissolved by n-Butyl Acetate. The components exposed to the highest wear rate can be coated with a hard, tough layer to prevent metal-to-metal contact, for instance graphite or molybdenum disulfide. (4) This is, however, very expensive and special ball bearings must be ordered.

It would probably be better to change the lubrication mode by preventing the fluid from surrounding the components in the motor and reducer. If the motor and reducer are placed in a separate container, only one rotating shaft must be connected to components outside this container (Figure 33). The passage in the container for

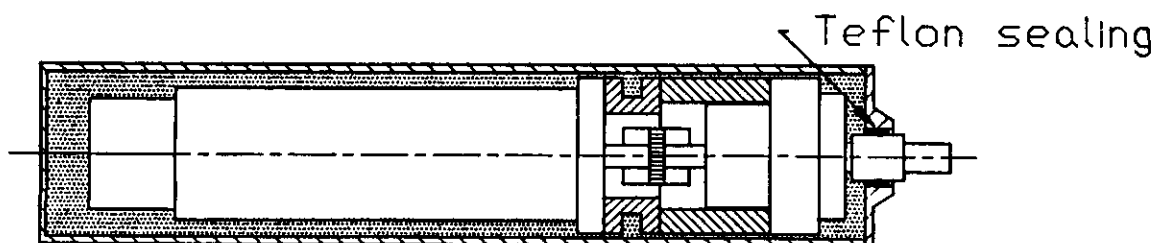


Figure 33. The motor and gear reducer placed inside a container to isolate them from n-Butyl Acetate.

this shaft can be sealed with Teflon seals. The maximum pressure difference between the inside of this container and the fluid in the drill hole is not supposed to be larger than about 30 MPa at a drilling depth of 3200 m. There are Teflon seals capable of sealing a passage against this pressure difference, but the container could be filled with another fluid at a higher pressure to reduce the pressure difference. If the pressure inside the container is higher than the pressure on the outside, no n-Butyl Acetate should flow into the container if a minor leakage should occur. It is desirable for the fluid inside the container to be a better lubricant than n-Butyl Acetate.

8. REFERENCES

1. Gosink, T.A., Tumeo, M.A., Koci, B.R., Burton, T.W.: A case for n-Butyl Acetate, a Safe, Auto-Dense Ice Coring Drilling Fluid, Fairbanks 1989, PICO (Polar Ice Coring Office) University of Alaska Fairbanks, TR 89-3, 20p.
2. Koci, B.R.: Evaluation of a prototype deep ice coring system, Fairbanks 1989, PICO (Polar Ice Coring Office) University of Alaska Fairbanks, TR 89-1, 44p.

3. Proenza, L.M., Kelley, J.J., Koci, B., Sonderup, J., Wumkes, M.: Shallow and deep ice coring devices developed by the Polar Ice Coring Office, Copenhagen 1990, PICO (Polar Ice Coring Office) University of Alaska Fairbanks, CP-90-2, 13p.
4. McGraw-Hill Encyclopedia of Science and Technology, McGraw-Hill Book Company, New York USA, 1987 6th edition, band 10 p.208-211.
5. Herrera, E.J., Gallardo, J.M.: Some case histories of wear-related failures of metallic materials, *Wear* 119 (1987) n.2 p.205-213.
6. Peterson, M.B., Winer, W.O.: Wear control handbook, American Society of Mechanical Engineers, 1980, p.283-311.
7. Scott, D.: Treatise on materials science and technology volume 13 Wear, Academic Press, New York, 1979, p.13-19, 66, 259-285.
8. Szeri, A.Z.: Tribology: Friction, lubrication and wear, Hemisphere Publishing Corporation, USA, 1980, p.510-518.
9. Lim, S.C., Ashby, M.F.: Wear-mechanism maps, *Acta Metall* 35 (1987) n.1 p.1-24.
10. Lim, S.C., Ashby, M.F., Brunton, J.H.: Wear rate transitions and their relationship to wear mechanisms, *Acta Metall* 35 (1987) n.6 p.1343-1348.
11. Chetwynd, D.G., McKee, F.A., Wride, C.H.: The measurement of wear damage, *Proceedings of the Institution of Mechanical Engineers (Part C)*, 201 (1987) n.4 p.251-258.
12. Graham Company: Graham Circulute Reducer, New 60 Series Catalog 9150, Graham Company, Milwaukee, Wisconsin, USA, 1987.
13. Marti, Max; Shimpco Drives, 9064 N. Deerbrok Trail, Brown Deer, Wisconsin 53223, USA, (414)-362-6900.
14. Boresi, A.P., Sidebottom, O.M.: Advance mechanics of materials, John Wiley & Sons, New York, 1985, p.629-631.

APPENDIX 1. THE MOTOR AND THE GEAR REDUCER

THE MOTOR

The motor used in this study was a Honeywell DC-servo motor with an output of 1 HP (745.7 Watts) at a speed of 1800 RPM, 180 Volts DC and 4.5 Amps. This type of motor is usually used in dry drill-holes but has also been used without any problems in holes filled with water. This is a brush type permanent magnet motor with an integral tachometer. The tachometer is a DC generator that produces a voltage which is proportional to the rotation speed of the motor. Electric motors usually have an efficiency of about 98%.

GEAR REDUCER

Operating Parts

The main power transmitting components in the reducer are a circulate wheel [1], an eccentric roller bearing [2], a set of internal pins [3] and a set of carrier pins [4]. The eccentric roller bearing on the input shaft [2] drives the wheel around the internal pins in an eccentric motion. The carrier pins and the bushings [6] transmit the power from the wheel to the output shaft [7] (Figure 1.1).

The circulate wheel, bushings and the internal pins are made from a high carbon (1%), high chromium (1.45%) bearing steel. The carrier pins are made from a low carbon chrome-molybdenum steel: 0.15% C, 0.75% Mn, 1.05% Cr and 0.22% Mo. The chrome-molybdenum ratio resembles that of steel SIS 2216 (Swedish Standard) with 0.15% C, 0.75% Mn, 1.0% Cr and 0.35% Mo. Steel SIS 2216 has a yield stress at about 280 MPa.

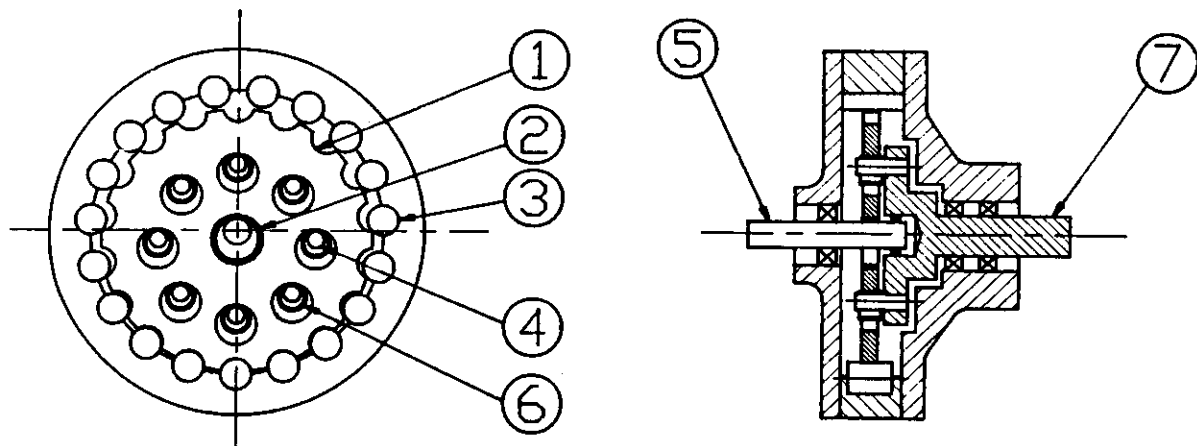


Figure 1.1. The circulate reducer.

Operating Principles

When the input shaft has completed one rotation, the eccentric roller bearing has also rotated once in the same direction. The eccentric bearing forces the circulate wheel to revolve around the internal pins in an eccentric motion. If the number of teeth on the wheel are less than the number of internal pins, the wheel has to rotate in the opposite direction around its own axis. How much the wheel has rotated depends on the difference between the number of teeth and number of internal pins. For example, if the difference in number of teeth and pins is 1, the wheel rotates 1 tooth pitch in the opposite direction (Figure 1.2). The output shaft is connected to the wheel by the carrier pins and the bushings. The reduction ratio can be expressed as:

$$R = (N-M) / M$$

where R = Reduction ratio

N = Number of internal pins

M = Number of teeth

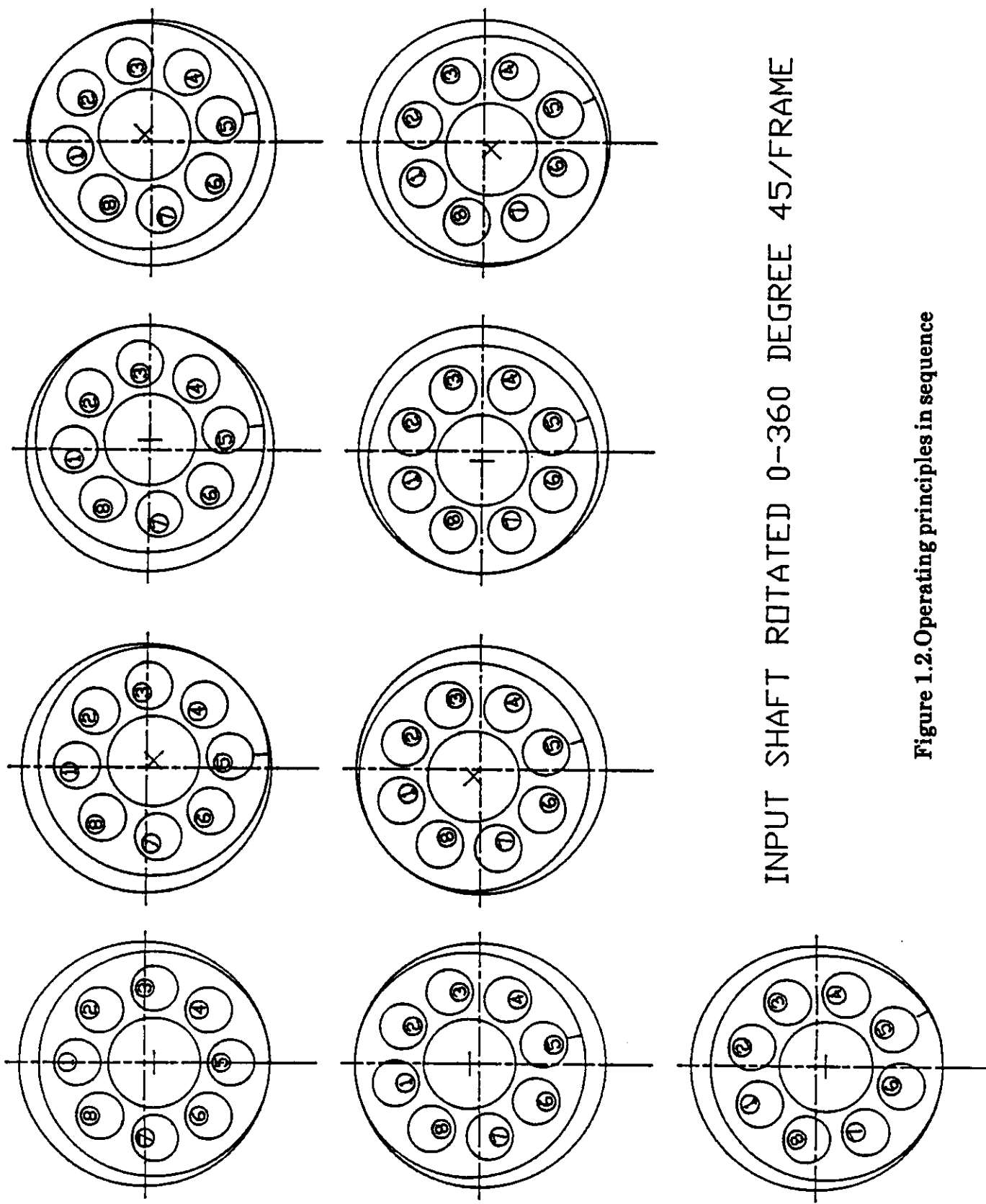


Figure 1.2. Operating principles in sequence

Technical data:

The technical data on the Circulate reducer according to the Graham Company Catalog (13) are:

Model number:	60 A 11 R
Lubrication:	Grease
Net. Weight:	10 kg (20 lbs)
Diameter input shaft:	19.05 mm (0.75 inch)
Diameter output shaft:	22.225 mm (0.875 inch)
Reduction ratio:	11:1
Efficiency:	over 90%
Internal pins:	# 36
Circulate teeth:	# 33

Example of output at two different input powers:

Different operating variables:	Input power [W]:	
	954.5	708.4
Input speed [RPM]:	1750	1165
Output speed [RPM]:	159	106
Output torque [Nm]:	53.4	59.3

The internal part dimensions are shown in Figures 1.3 - 1.7.

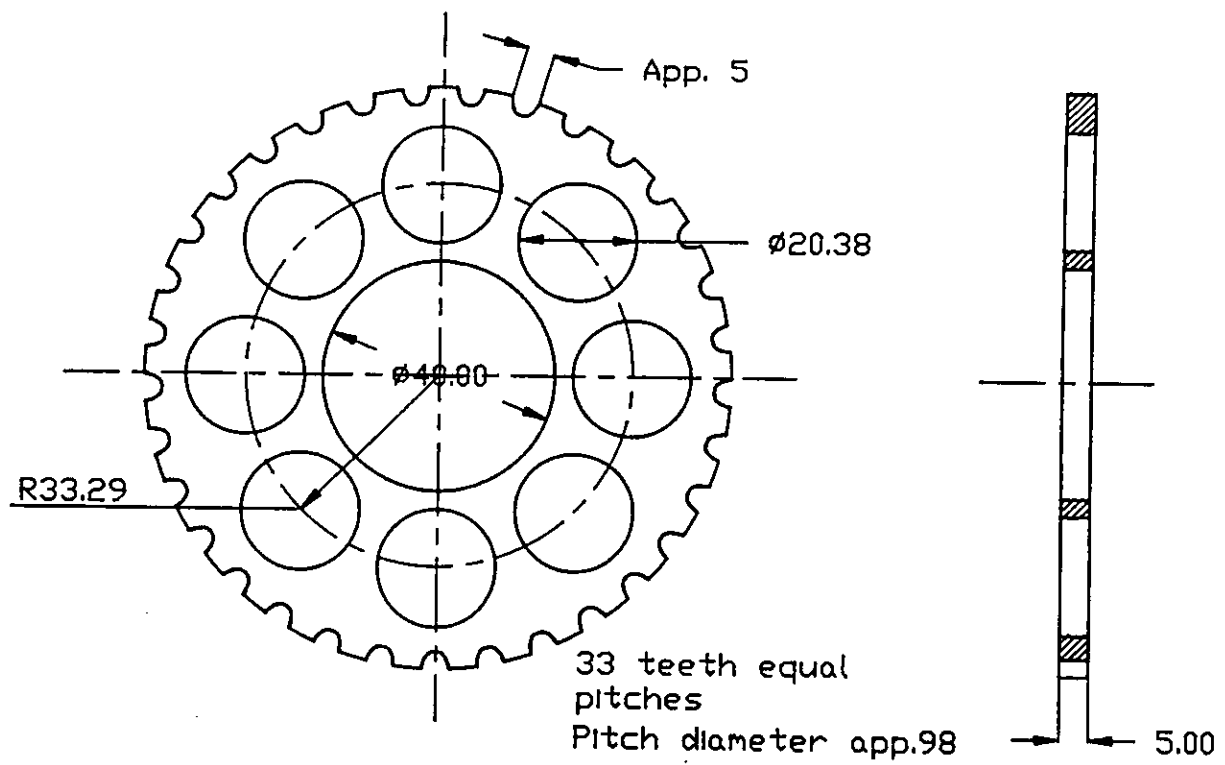


Figure 1.3. Circulate wheel.

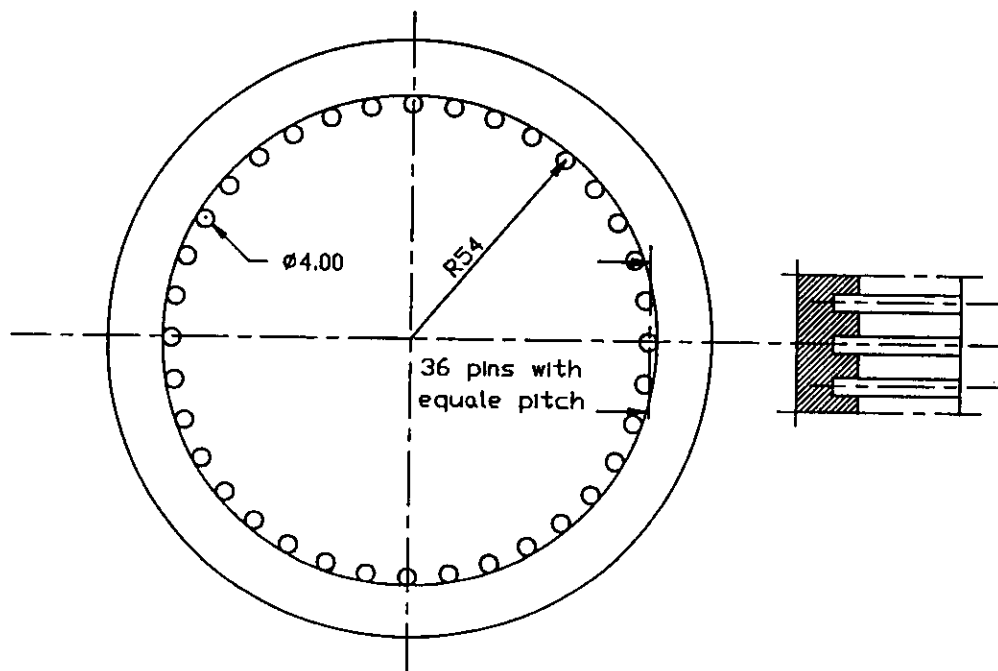


Figure 1.4. Internal pins.

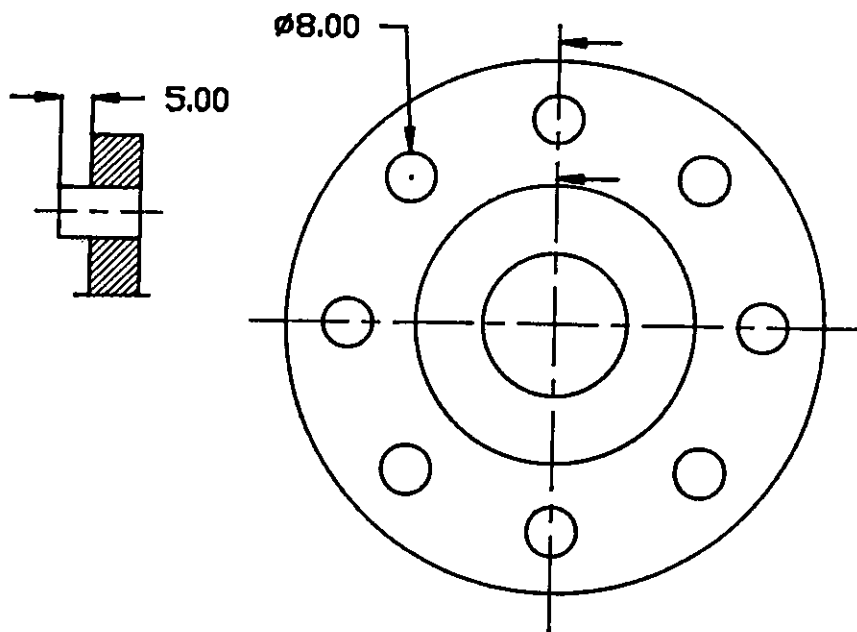


Figure 1.5. Output shaft with carrier pins.

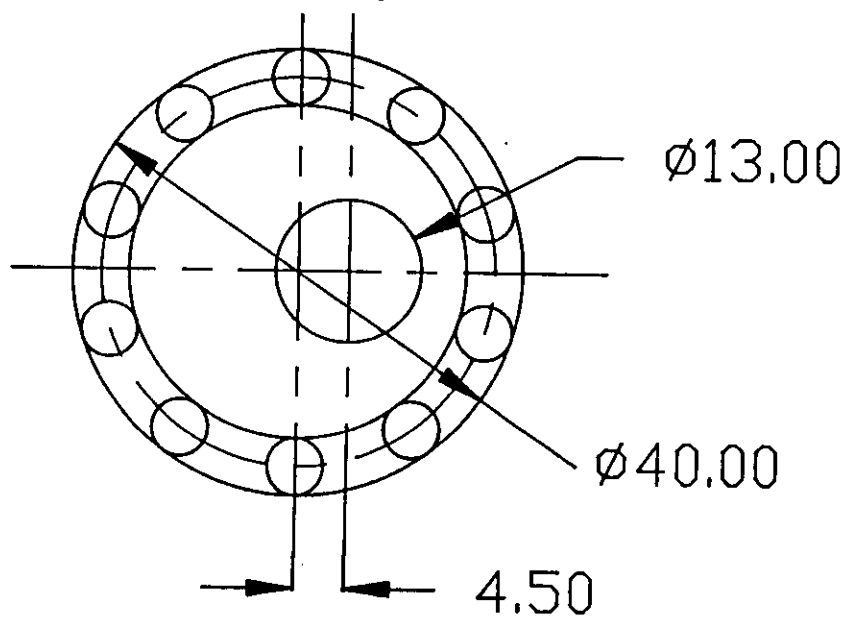


Figure 1.6. Eccentric roller.

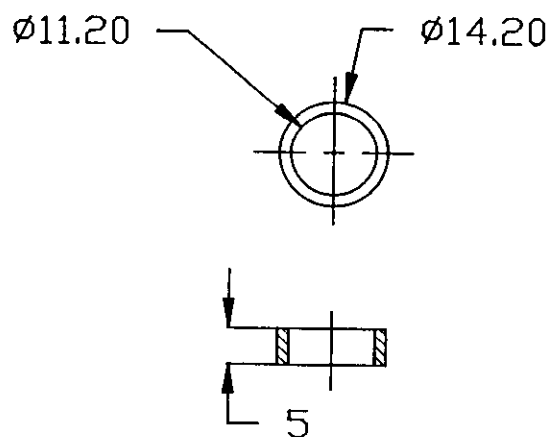


Figure 1.7. Bushings bearing.

APPENDIX 2. MONITORING DEVICES

The following devices were used to measure different quantities:

TORQUE:

Strain indicator

Vishay Instruments

Model P-350 AK, Serial number: 20167

Resolution: 2 μ strains

SPEED OF ROTATION:

Digital Multimeter

Fluke Mfg. Co., Inc.

Everett, Washington, USA

Model 8010A, Serial number: 3715332

Resolution: 0.1 volt

Digital Hand Tachometer

Herman H Sticht Co., Inc.

New York, USA

Model DH-1M, Serial number: 79316

Resolution: 1 RPM

Strip Chart Recorder

Hewlett Packard

Model 7402A-05-08 Recorder

Serial number: 1638A02411

TEMPERATURE:

Digital Thermometer, temp scale Fahrenheit

John Fluke Mfg. Co., Inc.

Seattle, Washington, USA

Model 2100A, Serial number: 30058

Resolution: 0.1 F

Multipoint Switch Unit

John Fluke Mfg. Co., Inc.

Model 2150A, Serial number: 28520

MICROMETER:

Swiss Precision Instruments, Inc.

Los Angeles, California, USA

Model 687, Serial number: 10-871-2

Resolution: 0.001 mm

DIRECT CURRENT CONVERTER:

Allen-Bradley

Milwaukee, Wisconsin, USA

Model 346

Resolution: 2 volts, 0.5 Amperes

WEIGHT:

Digital scale

Brainweigh B 300 D

OHAUS Scale Corp.

Florham Park, New Jersey, USA

Serial number P/N 75074-00

Resolution: 0.01 g

CALIBRATION OF THE TACHOMETER

To create a calibration curve for the DC tachometer, the rotation on the motor was measured both by a DC tachometer and a hand tachometer. The result was the following correlation between voltage and revolutions per minute:

$$[\text{RPM}] = 25.75 * [\text{V}]$$

CALIBRATION OF THE STRAIN INDICATOR

The torque on the brake shaft was obtained as a correlation between the loaded torque and the strain on the shaft's surface. The strain of the shaft was measured by a strain indicator.

The shaft was loaded by weights on a lever during the calibration. When only the lever was attached to the shaft, the reading on the strain indicator was 62 μStrain . A curve was created when torque was increased by adding weights. The correlation between the added torque (Nm) and the readings on the strain indicator (μStrain) was:

$$[\text{Nm}] = 0.0578 * ([\mu\text{Strain}] - 62) \text{ (The original curve)}$$

To create the calibration curve, the original curve was moved parallel until the point (0,0) was on the curve.

[V]	0	7.1	14.9	22.4	30.5	37.7	45.7	53.3
[RPM]	0	183	382	575	785	974	1181	1379
[RPM]=k*[V]	0	182.8	378.5	576.8	785.4	970.8	1176.8	1372.5

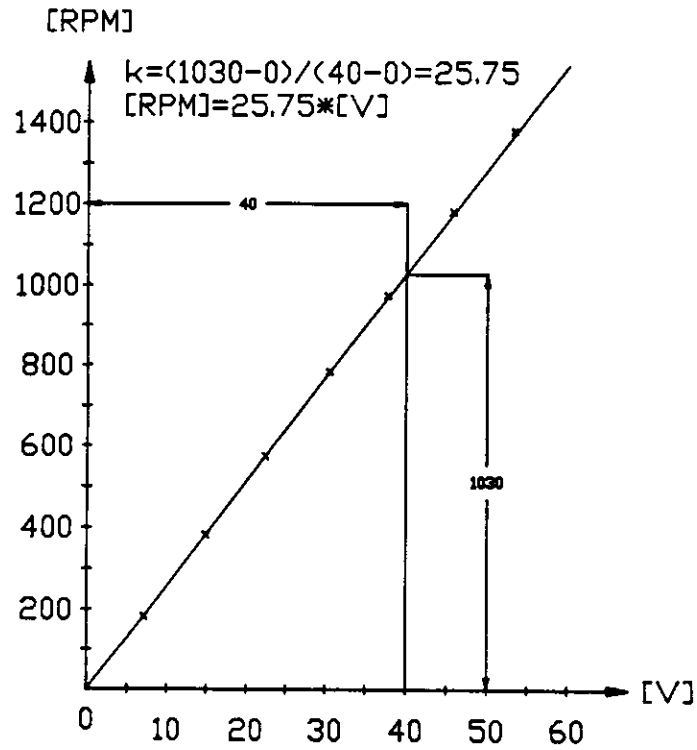


Figure 2.1. Calibration curve for the DC tachometer.

The correlation between the loaded torque (Nm) and the readings on the strain indicator (μ Strain) was:

$$[Nm] = 0.0578 * [\mu Strain] \text{ (The calibration curve)}$$

Weight [kg]	0	2.835	2.835	2.835	2.835	2.835	2.835	2.835	2.835	5.018	5.018	5.018	5.018	5.018
Length [m]	0	0.1524	0.2413	0.3302	0.4064	0.5461	0.7112	0.8636	0.3937	0.5080	0.6223	0.5715	0.6477	
Addmon [Nm]	0	4.24	6.71	9.18	11.30	15.19	19.78	24.02	19.38	25.00	30.36	28.13	31.88	
[μStrain]	62	164	210	245	276	336	397	462	404	487	575	537	590	
[Nm] *	0	5.89	8.55	10.57	12.37	15.84	19.66	23.12	19.77	24.56	29.65	27.46	30.52	

* [Nm]=0.0578*([μStrain]-62)

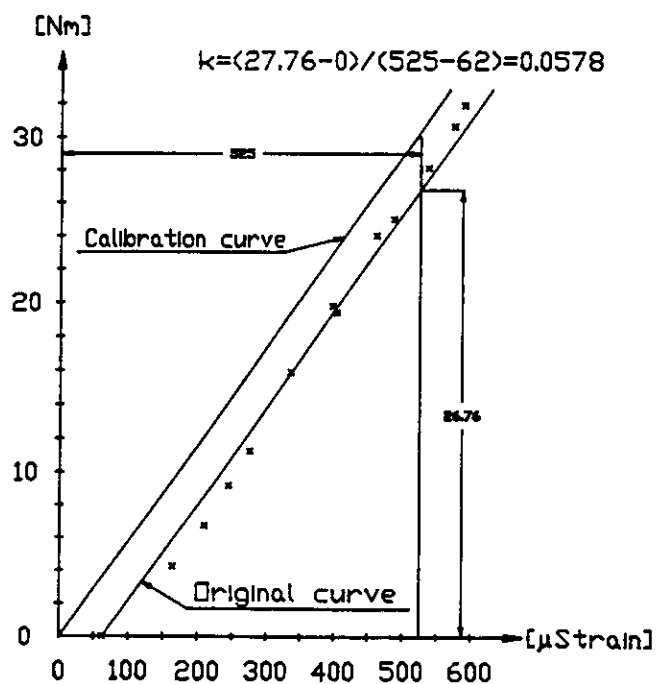


Figure 2.2. Original measuring curve and calibration curve for the strain indicator.

APPENDIX 3. CONSTRUCTION OF THE TEST STAND

THE CONTAINER

The container is an 18-inch-long trough made from 1/8-inch-thick steel plate. The thickness makes the trough torsionally stiff. Each end of the trough is open so that different end pieces can be used for other experiments. In this experiment we used two different end pieces, the first was a 1/2-inch-thick steel plate. The second one, where the brake is located, was made of a 1-inch-thick steel plate (Figure 3.1). Four supports were welded to the bottom of the trough. The motor and gear reducer system was fixed to the supports with two hose clamps.

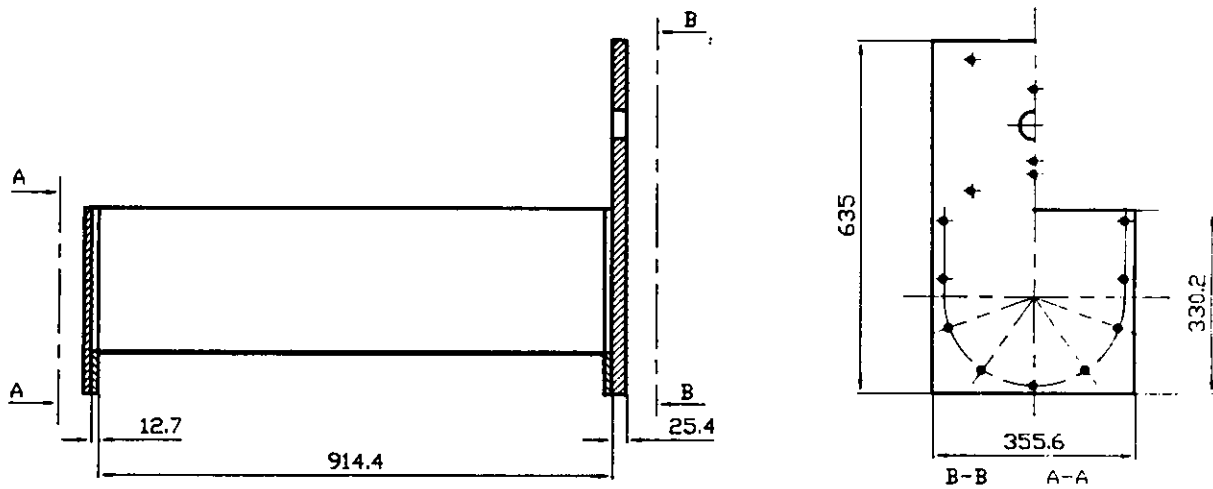


Figure 3.1. The trough with end pieces.

THE LOAD

To load the motor and gear reducer, an ordinary hydraulic disc brake from a motorcycle was used. Two different ways to operate the brake were used during the experiment.

The first method was to connect a motorcycle brake handle to the brake and load it with a spring (Figure 3.2). The problem with this method was that the handle leaked brake fluid. The leak caused the pressure in the hydraulic system to drop to almost 0 over a few hours and the load on the brake to decrease correspondingly.

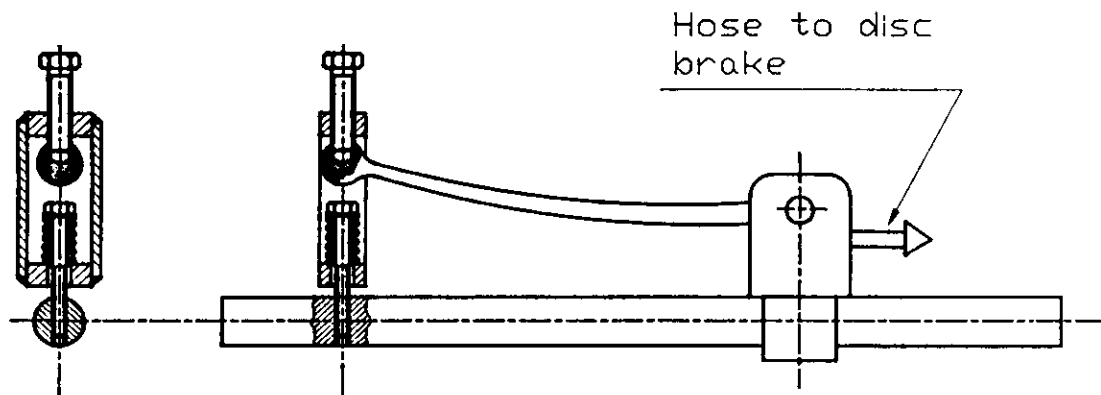


Figure 3.2. Motorcycle brake handle with spring.

The second method was to use compressed air to create the pressure in the hydraulic system (Figure 3.3). A tank with brake fluid was connected to the brake and the tank was placed under pressure with compressed air via a pressure regulator. The compressed air source was big enough to keep the pressure almost constant. Using this method, the torque on the brake shaft only varied between 28 and 32 Nm.

THE DISC BRAKE SHAFT

There was no shaft on the brake, so one had to be made. The hole in the disc had a diameter of $\phi_{\text{HOLE}} = 1.375$ in (34.9 mm). There was a standard key slot in the hole. The shaft was made of a cold drawn, round steel bar with a diameter of $\phi = 1.375$ in. and a length of 14 in.

To get better readings from the Wheatstone bridge the diameter had to be reduced on the section of the shaft where the strain gages were to be bonded. A brief calculation showed that a diameter of ϕ 20 mm would give accurate values.

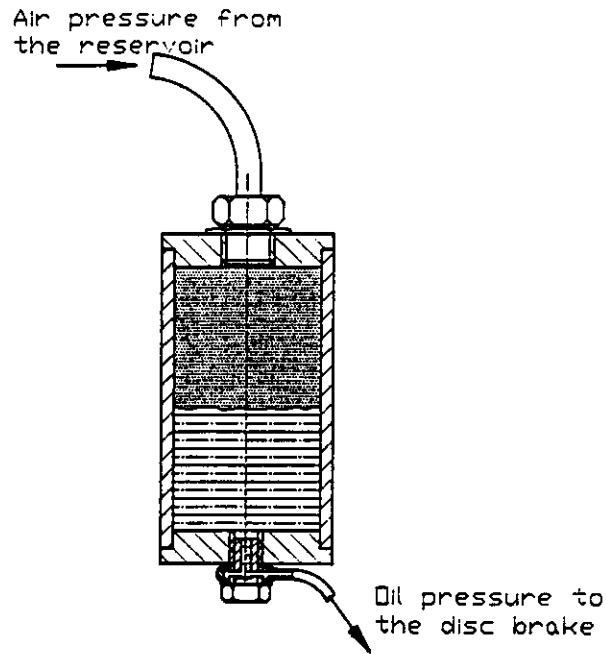


Figure 3.3. Compressed air brake.

A hole in the end of the shaft to accommodate the electronics plug from the bridge to the slip ring was needed. Two longitudinal slots were milled in the shaft to accommodate the strain gage wires and various keys and set screws for the components monitored on the shaft (Figure 3.4).

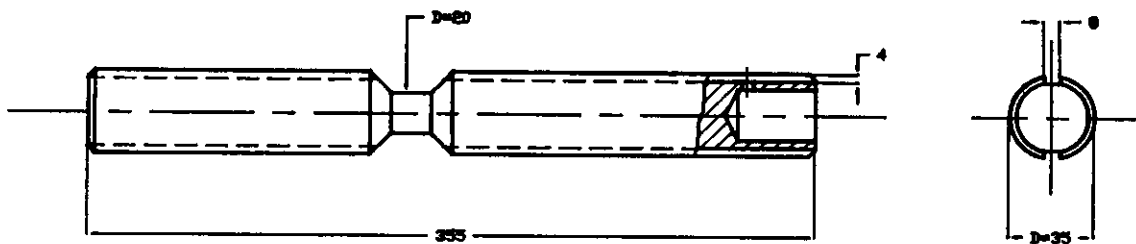


Figure 3.4. The brake shaft.

THE TRANSMISSION

The brake cannot operate in n-Butyl Acetate. To solve this problem, a chain drive connected the gear reducer with the brake shaft. An FMC Link-Belt standard roller chain (no 60 with a pitch of 0.75 in) was used together with two 14-tooth

sprockets (60 B14F with bores of 1.375 and 0.875 in). Both sprockets were attached with keys. To take up slack in the chain, a tensioner with a 13-tooth stock idler sprocket (60I13) was used (Figure 3.5).

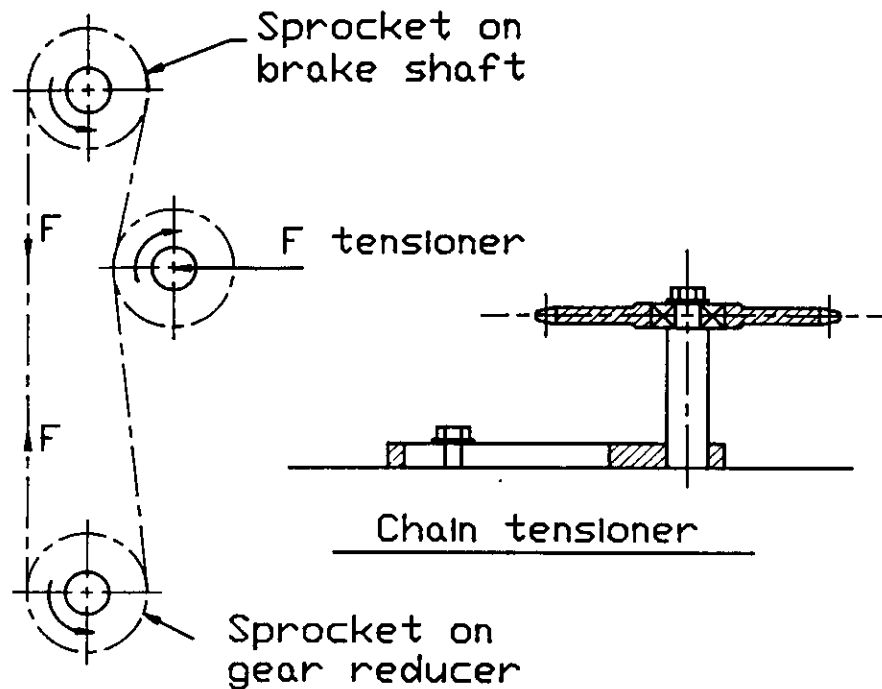


Figure 3.5. Chain tensioner with idler sprocket.

THE BEARINGS

To support the shaft, two FMC Standard Duty Ball Bearing Flange Units (FX3-U222H) for a shaft diameter of 1.375 in were used.

THE SLIP RING

To get the voltage into and the signal out from the Wheatstone bridge on the shaft, a standard slip ring type SSS was used. An adapter to connect the slip ring unit to the shaft is shown in Figure 3.6.

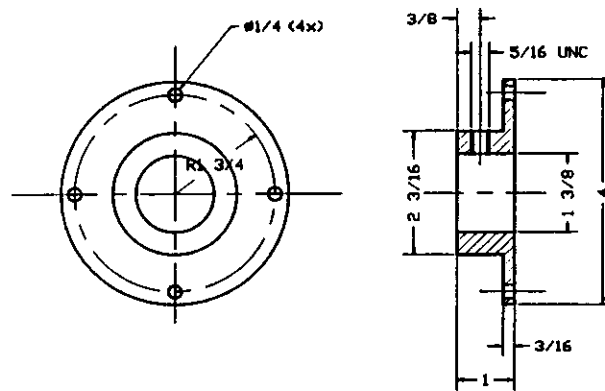


Figure 3.6. Adapter to fit the slip ring unit to the shaft.

THE COVERS

To protect the rotating parts of the chain drive and brake, two covers of plywood were made. Another cover was made to prevent the n-Butyl Acetate from evaporating.

APPENDIX 4. CHANGES IN WORKING CONDITIONS FOR THE MOTOR AND GEAR REDUCER SYSTEM

The following data were collected during 20 October - 3 November 1990 with equipment described in Appendix 2.

Acc. Time Hmin	Electrical input power			Loaded torque		Rotation	
	Voltage V	Current A	Power W	μ Strain	Nm	V	RPM
0	100	4	400	500	28.9	35	901
100	104	4	412	510	29.5	35	901
330	120	2	245	270	15.6	45	1159
330	100	4	400	520	30.1	35	901
500	120	1.5	180	200	11.6	46	1185
500	100	4	400	520	30.2	35	901
940	105	3.5	367	500	28.9	38	976
1140	112	3	336	-	-	40	1030
1140	100	4	400	520	30.1	35	901
1540	xxx	x	400	570	32.1	35	901
1540	100	4	400	500	28.9	37	953
2100	126	1	126	80	4.6	48	1236
2100	100	4	400	500	28.9	35	901
2115	102	4	408	500	28.9	37	953
2515	128	1	128	80	4.6	48	1236
2515	100	3.5	350	480	27.7	36	927
2630	94	5	470	690	39.9	32	824
2930	96	4	384	570	32.9	33	850
2930	100	4	400	500	28.9	33	850
3200	94	6	564	670	38.7	30	785
3200	100	4	400	500	28.9	35	901
3515	97	4.5	437	710	41.0	33	850
4640	124	1	124	80	4.6	47	1210
4640	100	4	400	500	28.9	35	901
5045	116	1.5	174	210	12.1	43	1107
5045	100	4	400	500	28.9	35	901
5545	110	2	220	320	17.6	40	1030
5545	100	4	400	500	28.9	35	901
6100	117	1.5	176	210	12.1	43	1115
6100	100	4	400	520	30.1	35	901
7100	124	1	124	110	6.4	45	1159
7100	100	4	400	500	28.9	35	901
7200	124	1	124	110	6.4	47	1210
7200	100	4	400	510	29.5	35	910
7810	100	3.5	350	440	25.4	36	927
7900	83	25	2075	0	0	0	0

Ack. Time Hmin	TEMPERATURES °F ([°C] = ([°F] - 32) / 1.8)			
	Surrounding air	n-Butyl Acetate bath	Gear Reducer	Motor
0	12.2	19.7	22.1	22.2
100	12.9	32.7	34.4	34.6
330	23.2	54.4	55.9	56.2
500	30.2	66.0	6.4	67.6
940	25.3	71.6	74.7	74.8
1140	25.1	67.8	70.7	70.7
1140	16.8	18.4	18.6	18.7
1540	18.9	53.3	56.8	57.0
2100	22.8	49.6	50.4	52.0
2515	24.1	50.4	51.4	52.9
2515	20.3	19.8	20.8	21.3
2630	21.3	41.2	44.6	45.9
2930	23.8	53.0	56.1	57.4
2930	24.3	49.8	52.2	55.0
3200	21.9	68.0	73.1	75.8
3515	18.0	53.1	56.5	58.0
4600	25.9	35.8	36.9	38.0
5045	27.2	39.0	40.0	41.6
5545	27.2	46.0	48.6	49.4
6100	23.2	39.3	42.6	43.2
7100	15.8	30.4	31.7	34.1
7250	17.9	41.7	43.9	45.7
7810	18.1	61.3	67.5	66.9
7900	17.4	55.7	63.6	51.8

STOPS DURING THE FIRST PERIOD:

- 1140 Stop during the first night
- 2515 Stop during the second night
- 2930 Stop to allow adjusting of the cover for the moving parts

Acc. Time Hmin	Electrical input power			Loaded torque		Rotation	
	Voltage V	Current A	Power W	μ Strain	Nm	V	RPM
7900	101	3.6	364	500	28.9	34	888
7930	103	3.5	361	450	26.0	36	927
8010	100	4	400	500	28.9	34	888
8205	126	1	126	110	6.4	47	1215
8305	126	1	126	110	6.4	47	1215
8330	101	4	404	500	28.9	35	901
8510	106	3.6	382	500	28.9	37	953
9000	102	4	408	540	32.1	35	901
9400	102	4	408	540	32.1	35	901

Ack. Time Hmin	TEMPERATURES °F ([°C]=([°F]-32)/1.8)			
	Surrounding air	n-Butyl Acetate bath	Gear Reducer	Motor
7900	29.8	22.1	24.1	25.3
7930	21.1	25.0	27.4	28.8
8010	20.0	25.0	27.2	27.8
8010	21.1	23.0	23.8	24.3
8205	19.3	31.3	32.0	33.4
8325	18.5	32.0	33.7	34.8
8330	18.5	32.0	33.7	34.8
8510	7.6	42.7	45.3	46.3
8955	11.5	51.0	54.6	55.8

STOPS DURING THE SECOND PERIOD:

8010 Stop to allow adjusting the new brake

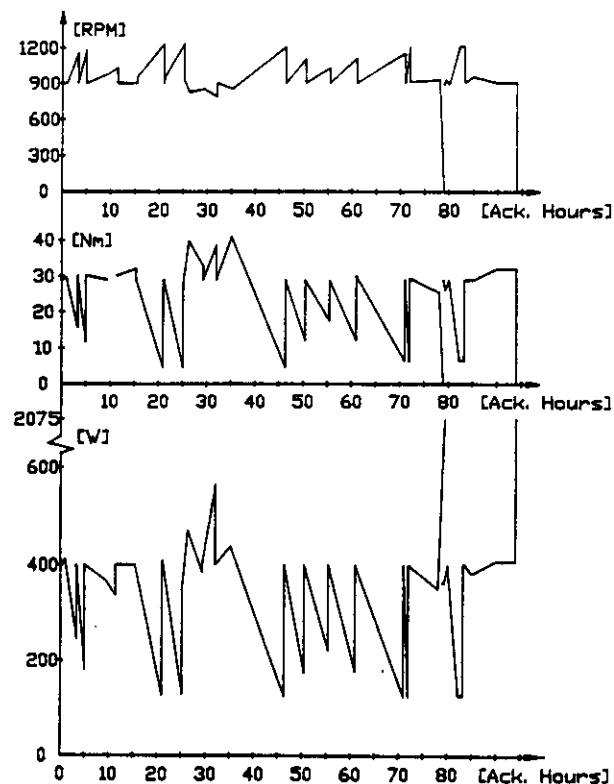


Figure 4.1. Changes in input power, loaded torque and rotation speed during the two periods.

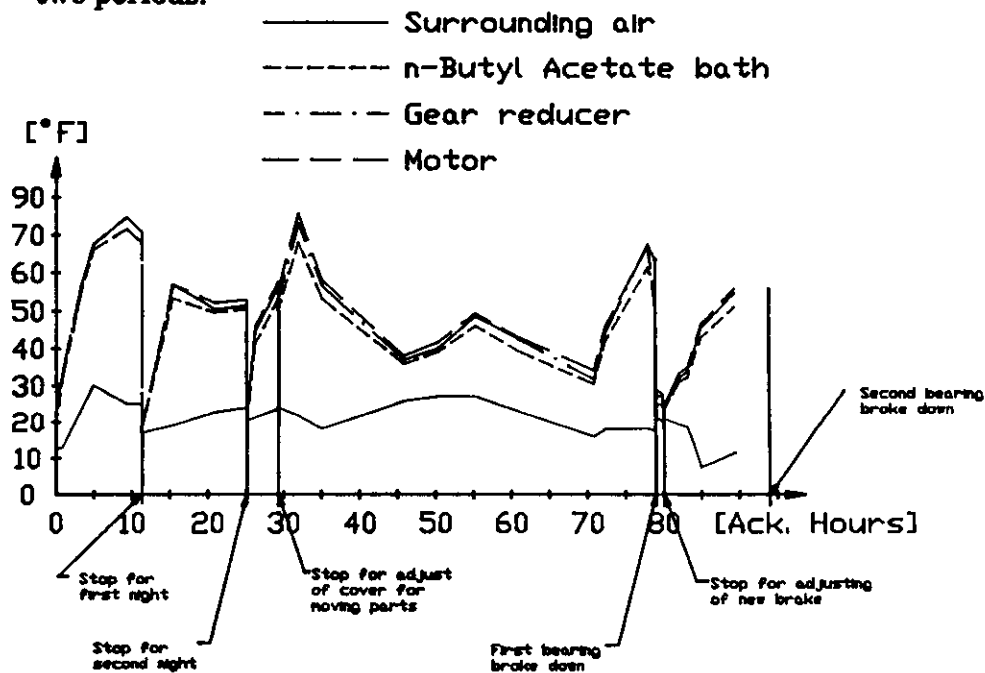


Figure 4.2. Changes in temperatures during the two periods.

APPENDIX 5. CHANGES IN ROTATION SPEED WHEN THE TEST SYSTEM BROKE DOWN

When the ball bearings failed, the shaft in the reducer froze. The changes in rotation were continually recorded by the strip chart recorder. The paper speed was 1mm/s and the voltage range 0-50 V.

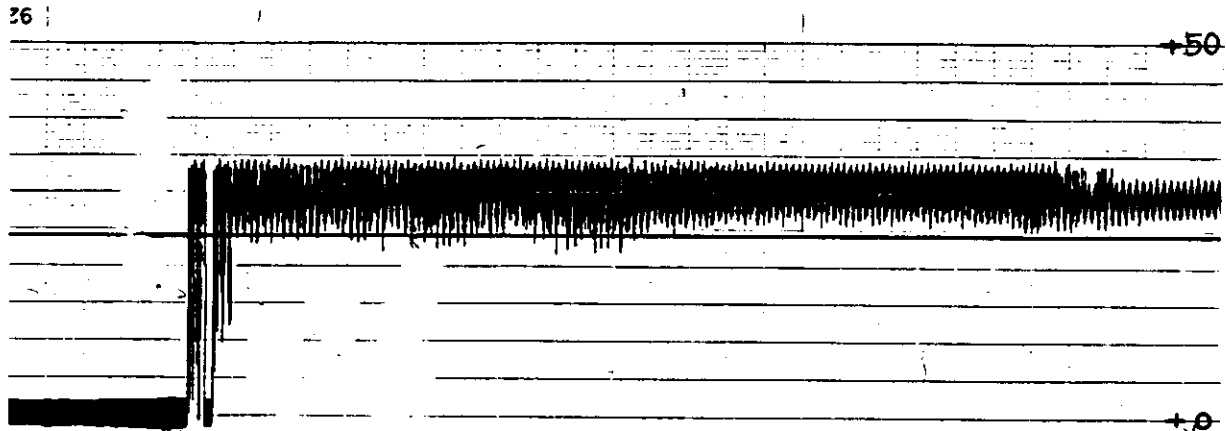


Figure 5.1. The change in rotation speed when the first bearing failed (79h) displayed on the strip chart.

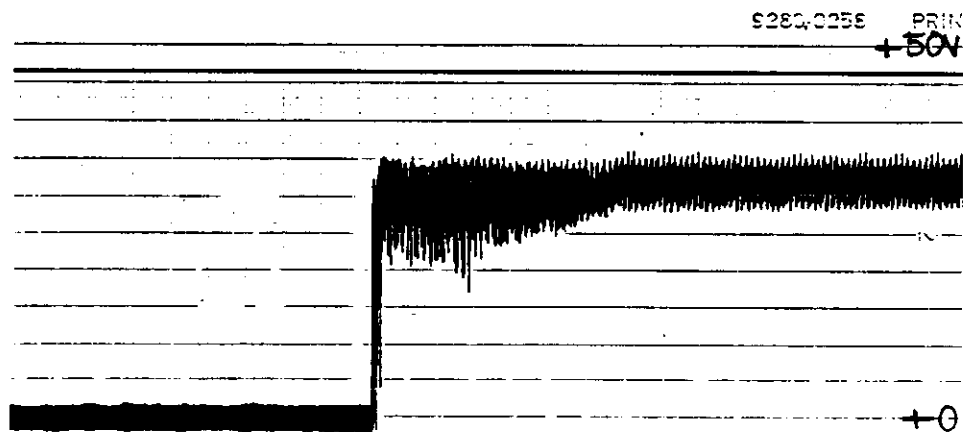


Figure 5.2. The change in rotation speed when the second bearing failed (94h) displayed on the strip chart.

APPENDIX 6. ROTATION SPEED AND LOAD IN THE GEAR REDUCER.

ROTATION SPEED

The output speed from the motor during the test was approximately 900 RPM when the system was loaded and 1200 when idling. Figure 6.1 shows the rotation speed of different parts in the reducer when the system is running with load and when it is idling.

Speed of:	name:	Formula:	Speed: * [RPM]/[rad/s]
Input shaft	n_{in}	---	900/94.25 (1200/125.6)
Output shaft	n_{out}	$-n_{in}/11$	-82/-8.59 (-110/-11.52)
The wheel	n_{wheel}	n_{out}	-82/8.59 (-110/11.52)
The housing	n_{house}	---	0/0 (0/0)
Bearing 1 inner ring	n_{1in}	n_{in}	900/94.25 (1200/125.6)
Bearing 1 outer ring	n_{1out}	n_{in}	0/0 (0/0)
Bearing 1 in-rel.out-ring	n_1	$n_{1in}-n_{1out}$	900/94.25 (1200/125.6)
Bearing 2 inner ring	n_{2in}	n_{in}	900/94.25 (1200/125.6)
Bearing 2 outer ring	n_{2out}	n_{out}	-82/-8.59 (-110/-11.52)
Bearing 2 in-rel.out-ring	n_2	$n_{2in}-n_{2out}$	982/102.83 (1310/137.18)
Bearing 3 inner ring	n_{3in}	n_{out}	-82/-8.59 (-110/-11.52)
Bearing 3 outer ring	n_{3out}	n_{house}	0/0 (0/0)
Bearing 3 in-rel.out-ring	n_3	$n_{3in}-n_{3out}$	-82/-8.59 (-110/-11.52)
Bearing 4 inner ring	n_{4in}	n_{out}	-82/-8.59 (-110/-11.52)
Bearing 4 outer ring	n_{4out}	n_{house}	0/0 (0/0)
Bearing 4 in-rel.out-ring	n_4	$n_{4in}-n_{4out}$	-82/-8.59 (-110/-11.52)

* Speed in brackets is when the system is idling.

Figure 6.1. The speeds in the reducer as a function of the speed of the motor.

IN- AND OUTPUT TORQUE, GEAR REDUCER

The input power during drilling is between 200 and 600 W, 200 when the drilling is started and 600 watts at the end of each core sample when the well screen is full. In this study the input power was initially adjusted to a mean value of 400 W at a motor speed of 900 RPM. Unfortunately, due to leakage of brake oil this value was not maintained throughout the experiment. The expression for the input torque to the reducer can be described as:

$$M_{in} = (e_{motor} * P_{Ein} * 60) / (2 * \pi * n_{in}) \quad (A)$$

Where: M_{in} [Nm] (Input torque to the reducer)
 $e_{motor} = 98 \%$ (The efficiency of the motor)
 $P_{Ein} = 400$ [Watts] (The input power to the motor)
 $n_{in} = 900$ [RPM] (The speed of the motor)

If these values are used in the formula above (A), the input torque will be:

$$M_{in} = 4.16 \text{ [Nm]} \quad (1)$$

According to the manufacturer, the efficiency of the reducer is better than 90%. The efficiency was assumed to be about 90%, but it will probably be less due to lack of lubrication. The expression for the output torque can be described as:

$$M_{out} = (e_{motor} * e_{reducer} * P_{Ein} * 60) / (2 * \pi * n_{out}) \quad (B)$$

Where: M_{out} [Nm] (Output torque from the reducer)
 $n_{out} = 82$ [RPM] (Output speed from reducer)

If these values are used in the formula above (B) the output torque will be:

$$M_{out} = 41.1 \text{ [Nm]} \quad (2)$$

ESTIMATION OF FORCES ACTING IN THE CONTACTS WHEEL-BUSHINGS-CARRIER PINS

In Figure 6.2, the forces acting in the contacts between the carrier pins, bushings and the wheel are shown. The marked parts show the theoretical zone on the carrier pins and on the circulate wheel that distribute the torque.

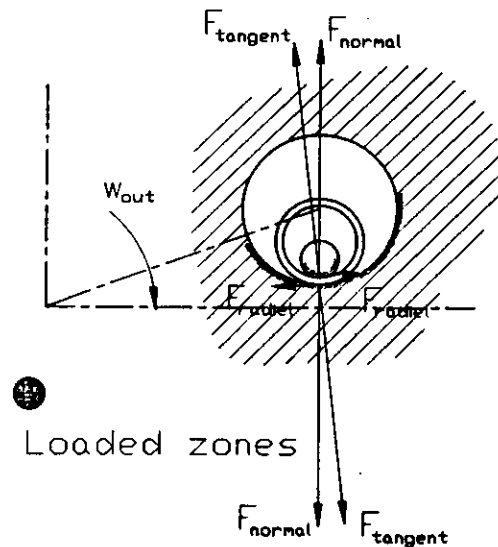


Figure 6.2. Forces and loaded zones in the contacts between wheel, bushings and carrier pins.

The carrier pins distributing the torque are the ones that are in contact with the wheel in the same direction as the torque is acting. In Figure 6.3a it will be pins number 1-4 and in Figure 6.3k, pins number 2-5. Assume the contact force is equal for all pins in contact. The torque acting inside the reducer is not affected by the efficiency ratio, that means the output torque from the reducer has to be divided by $e_{reducer}$. The contact force can be estimated as:

$$F_{carr} = M_{out} / (4 * R * e_{reducer}) \quad (C)$$

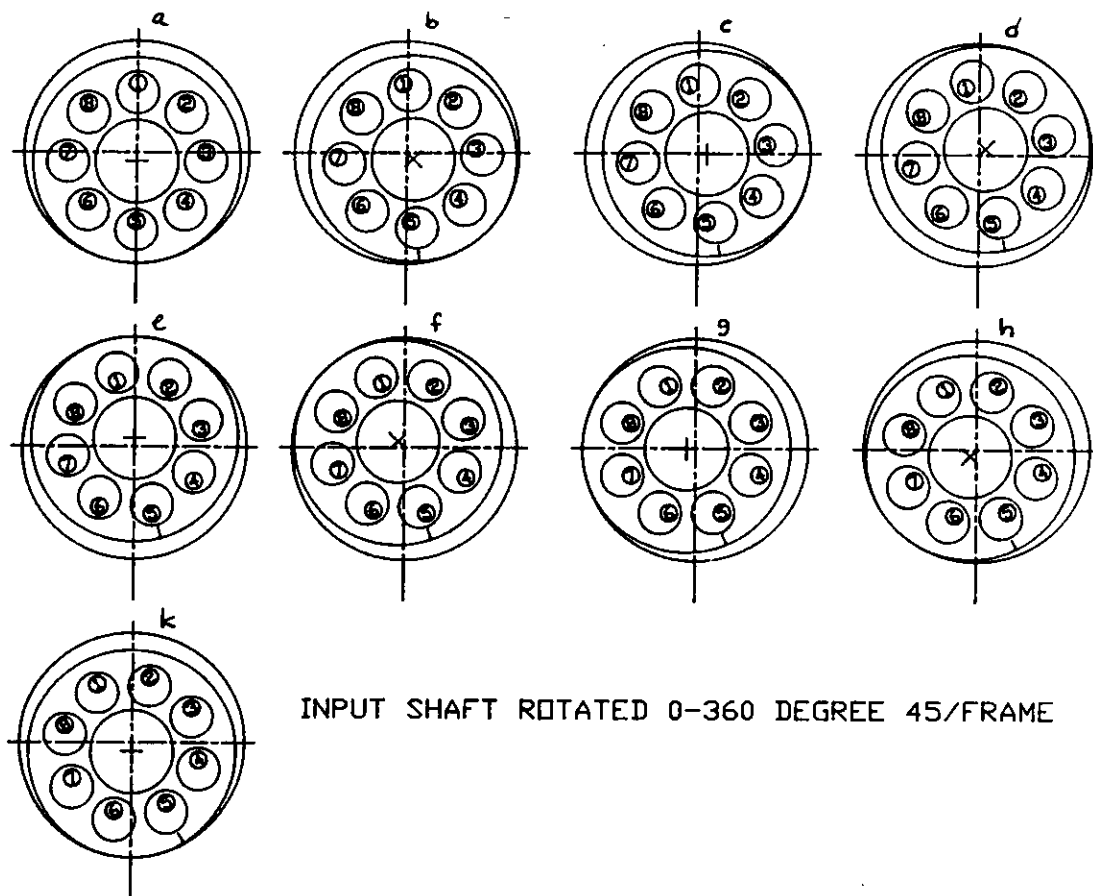


Figure 6.3. Operation principles.

Where:	F_{carr}	[N]	(Force acting in the normal direction to the surface.)
	R	$= 33.25$ [mm]	(Distance from the center of the output shaft to the center of the carrier pins.)
	M_{out}	$= 41.1$ [Nm]	(Output torque from the reducer.)
	$e_{reducer}$	$= 90\%$	(Efficiency of the reducer)

If these values are used in the formula above (C), the normal force will be:

$$F_{carr} = 343 \text{ [N]} \quad (3)$$

WHEEL - INTERNAL PINS

It is hard to know how many internal pins are in contact with the wheel and are able to transmit the force at any given time. An estimation is that there are about four of them in contact on average. Using formula (C) and the values below for an approximation:

where:	F_{int}	[N]	(Force acting in the normal direction to the surface)
	R	$= 54 \text{ [mm]}$	(Distance from the center of the output shaft to the center of the internal pins)
	M_{out}	$= 41.1 \text{ [Nm]}$	(Output torque from the reducer)

The normal force will be estimated to:

$$F_{int} = 211 \text{ [N]} \quad (4)$$

SLIDING VELOCITIES

WHEEL-CARRIER PINS

The sliding velocity between the surfaces of the wheel and the carrier pins is interesting. In Figure 6.4, the directions of the velocities are shown. The surface velocity of the carrier pins and the hole in the wheel can be estimated as:

$$v_{carrier \text{ pin}} = w_{out} * r_1$$

$$v_{wheel} = w_{out} * r_2 - w_{in} * r_3$$

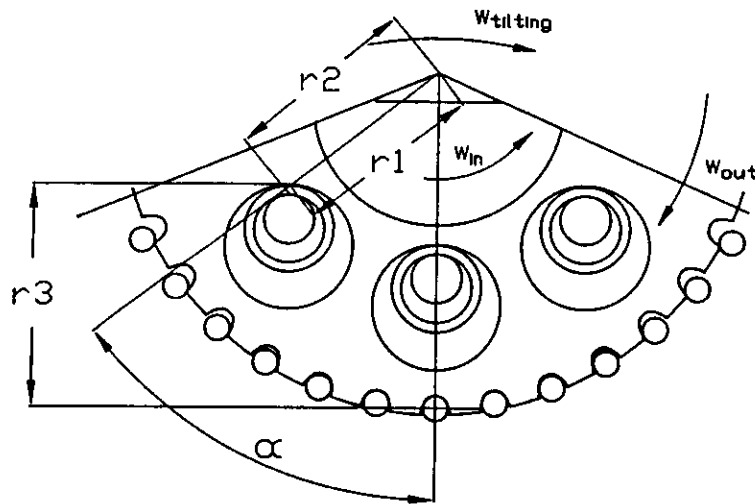


Figure 6.4. Velocities of the wheel and carrier pins.

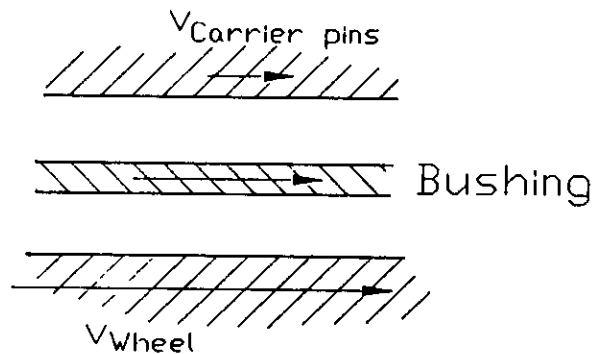


Figure 6.5. Sliding motion between wheel, bushing and carrier pin.

Where	w_{out}	=	8.59 [rad/s]	(Output speed from the reducer)
	w_{in}	=	94.25 [rad/s]	(Input speed to the reducer)
	r_1	=	$f(\alpha)$ [m]	(Distance from center of reducer to contact point)
	r_2	=	$r_1 + t$ [m]	
	r_3	=	$f(\alpha)$ [m]	(Distance from contact between wheel and internal pins)
	t	=	$1.5E-3$ [m]	(Thickness bushings. Angle between contact wheel-internal pins and wheel - bushing - carrier pins)

The relative velocity between the carrier pins and the wheel can be estimated as:

$$v_{rel} = |v_{wheel} - v_{carrier\ pins}|$$

A calculation of the relative velocity between the wheel and the carrier pin, as a function of the distance to the contact between the wheel and internal pins, results in:

$\alpha[^\circ]$	$v_{rel} [m/s]$
0	2.3
90	4.5
180	7.7

WHEEL-INTERNAL PINS

The sliding velocity between the wheel and the internal pins can be estimated as (Figure 6.6):

$$v_{pin} = (w_{in} * r_{pin}) - (w_{pin} * r_{pin})$$

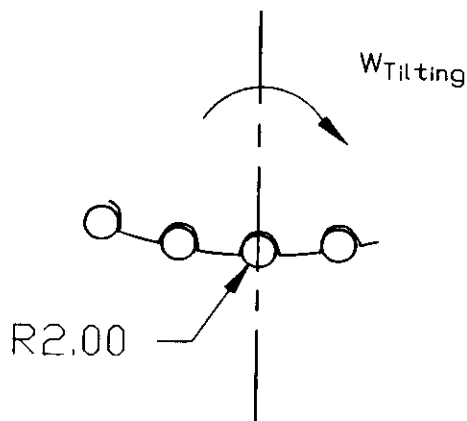


Figure 6.6. The relative sliding motion between the wheel and internal pins.

where v_{pin} [m/s] (Relative sliding velocity)
 $r_{pin} = 2e-3$ [m] (Radius of internal pin)
 $w_{in} = 94.25$ [rad/s] (Input speed to the reducer)
 $w_{pin} = 0$ [rad/s] (Speed on internal pins)
 $v_{pin} = 0.19$ [m/s]

LOADS ON BEARINGS

Figure 6.7 shows the placements of bearings in the reducer and the load on each of them.

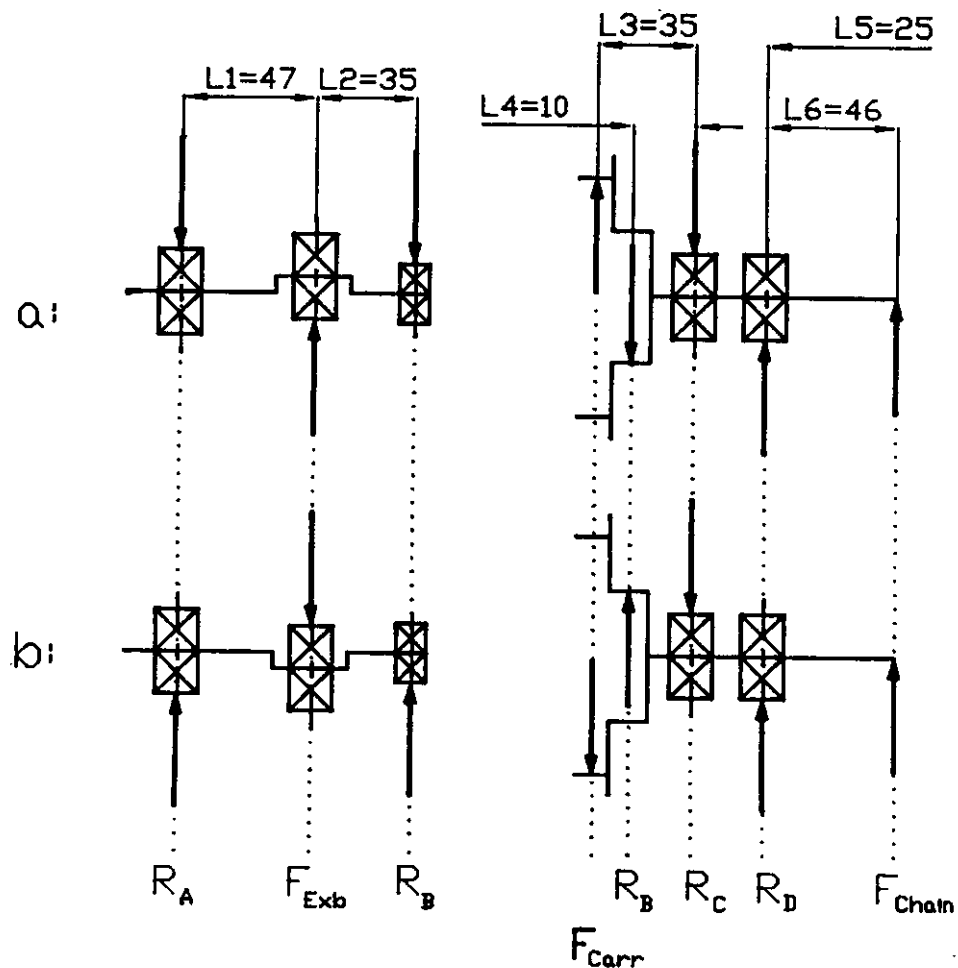


Figure 6.7. Locations of bearings and their forces in the reducer.

F_{chain} is the tension in the chain. It can be estimated at:

$$F_{chain} = M_{out} / R_{sprocket}$$

Where: $M_{out} = 41.1$ [Nm] (Output torque from the reducer)

$R_{sprocket} = 42.8$ [mm] (Pitch radius on sprocket)

$$F_{chain} = 960 \text{ [N]}$$

The force F_{carr} can be estimated as:

$$F_{carr} = 4 * F$$

$$F_{carr} = 1372 \text{ [N]}$$

The forces acting on the wheel are shown in Figure 6.8, R_{exb} can be estimated as:

$$F_{exb} = 4 * F_{int} - F_{carr}$$

Where: F_{int} can be approximated to:

$$F_{int} = 211/\sqrt{2} \text{ [N]} \quad (\text{An approximation of the force component, acting in the same direction as } F_{carr})$$

$$F_{exb} = -775.2 \text{ [N]}$$

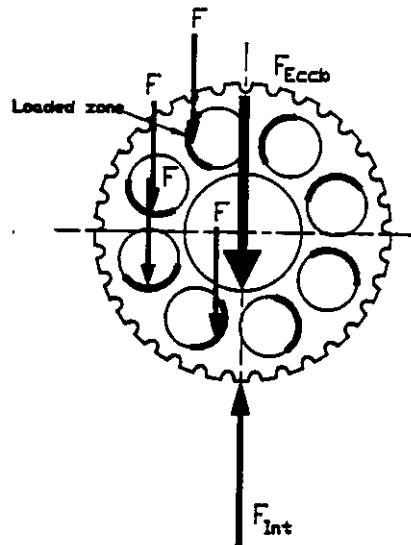


Figure Figure 6.8. Forces acting on the circulate wheel.

From this, the reaction forces in the bearings can be estimated as:

$$R_A = -F_{\text{exb}} * L_2 / (L_1 + L_2)$$

$$R_B = F_{\text{exb}} - R_A$$

$$R_C = (F_{\text{carr}}(L_3 + L_5) + R_B(L_4 + L_5) - F_{\text{sprocket}} * L_6) / L_5$$

$$R_D = R_C - R_B - F_{\text{carr}} - F_{\text{chain}}$$

Force:		a:*	b:*
R _A	[N]	-331	331
R _B	[N]	-444	444
R _C	[N]	904	-4437
R _D	[N]	-983	-4469
R _{exb}	[N]	-775	-775

*See Figure 6.7

APPENDIX 7. CONTACT STRESSES ON COMPONENTS IN THE GEAR REDUCER

Approximate contact stresses are estimated according to A. Boresi and O. Sidebottom. (11) The contacts between the internal pins, circulate wheel, bushings and carrier pins (see Appendix 1) are narrow rectangular areas with the forces normally applied to the contact areas.

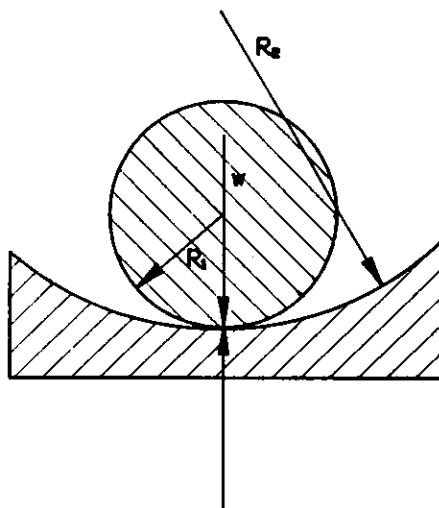


Figure 7.1. Line contact for a circular cylinder resting inside a larger hollow cylinder.

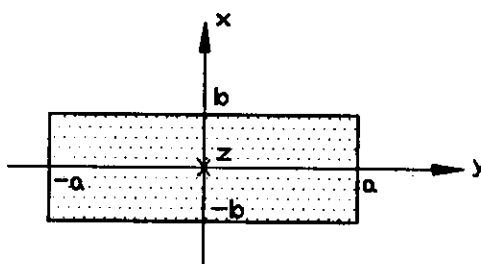


Figure 7.2. The contact area and the corresponding axis x, y and z.

The stresses for these contacts can be estimated at various distances below the surface (z):

$$\sigma_{yy} = -2\nu[(1 + (z/b)^2)^{1/2} - (z/b)] * b/D$$

$$\sigma_{xx} = - \left[\frac{((1 + (z/b)^2)^{1/2} - (z/b))^2}{(1 + (z/b)^2)^{1/2}} \right] * b/D$$

$$\sigma_{zz} = - [1 + (z/b)^2]^{-1/2} * b/D$$

$$b = (2wD/\pi)^{1/2}$$

$$D = \frac{1}{(1/2R_1) + (1/2R_2)} \left[\frac{1-\nu_1^2}{E_1} + \frac{1-\nu_2^2}{E_2} \right]$$

R_i are the radii of curvature (m) and w is the applied load per unit length of the area (N/m). For an ordinary steel:

$$E_i = 2.10 \cdot 10^{11} \text{ Pa} \quad (\text{Elastic modulus})$$

$$\nu_i = 0.3 \quad (\text{Poissons ratio})$$

The stresses for the various contacts are estimated for the center of the contact area at two different depths:

* on the surfaces ($z/b = 0$), where the maximum principal stresses ($\sigma_{yy,xx,zz}$) occurs:

$$\sigma_{yy} = -2\nu * b/D$$

$$\sigma_{xx} = -b/D$$

$$\sigma_{zz} = -b/D$$

$$\tau = \frac{1}{2} * (\sigma_{xx} - \sigma_{zz})$$

* at $(z/b) = 0.7861$, where the maximum shearing stress (τ) occurs:

$$\sigma_{yy} = -0.9718 * \nu b/D$$

$$\sigma_{xx} = -0.1856 * b/D$$

$$\sigma_{zz} = -0.7861 * b/D$$

$$\tau_{\max} = \frac{1}{2} * (\sigma_{xx} - \sigma_{zz}) = 0.300 * b/D$$

The radii of curvature and length of the contacts are displayed in Appendix 1 and the normal applied forces in Appendix 6.

CONTACT	R ₁ (mm)	R ₂ (mm)	F(N)	2a(mm)
BUSHING-C. WHEEL	7.1	-10.2	343	4.8
BUSHING-CAR. PINS	4.0	-5.6	343	4.8
C. WHEEL-INT. PINS	2.0	-2.4	211	4.8

CONTACT	w=F/2a (N/m)	D (m ³ /N)	b=(2wD/π) ^{1/2} (m)	Contact Area (m ²)
BUSHING-C. WHEEL	71.46*10 ³	404.95 * 10 ⁻¹⁵	135.73 * 10 ⁻⁶	1.30 * 10 ⁻⁶
BUSHING-CAR. PINS	71.46*10 ³	242.67 * 10 ⁻¹⁵	105.07 * 10 ⁻⁶	1.01 * 10 ⁻⁶
C.WHEEL-INT. PINS	43.96*10 ³	208.00 * 10 ⁻¹⁵	76.30 * 10 ⁻⁶	0.732 * 10 ⁻⁶

$$(z/b) = 0$$

CONTACT	σ_{xx} [MPa]	σ_{yy} [MPa]	σ_{zz} [MPa]	π [MPa]
BUSHING-C. WHEEL	-335.18	-201.11	-335.18	0
BUSHING-CAR.PINS	-432.97	-259.78	-432.97	0
C. WHEEL-INT.PINS	-366.83	-220.10	-366.83	0

$$(z/b) = 0.7861$$

CONTACT	σ_{xx} [MPa]	σ_{yy} [MPa]	σ_{zz} [MPa]	π_{max} [MPa]
BUSHING-C. WHEEL	-62.21	-97.72	-263.49	100.55
BUSHING-CAR. PINS	-80.36	-126.23	-340.36	129.89
C. WHEEL-INT.PINS	-68.08	-106.95	-288.37	110.05